Electronic Supplementary Material (ESI) for Physical Chemistry Chemical Physics.

SUPPLEMENTARY MATERIALS

3-D bond-paths of QTAIM and the Stress Tensor in Neutral Lithium Clusters, Li_m (m = 2-5), Presented on the Ehrenfest Force Molecular Graph

Alireza Azizi, Roya Momen, Steven R. Kirk* and Samantha Jenkins*

Key Laboratory of Chemical Biology and Traditional Chinese Medicine Research and Key Laboratory of Resource National and Local Joint Engineering Laboratory for New Petro-chemical Materials and Fine Utilization of Resources, College of Chemistry and Chemical Engineering, Hunan Normal University, Changsha, Hunan 410081, China

*email: samanthajsuman@gmail.com
*email: steven.kirk@cantab.net

1. Supplementary Materials S1. QTAIM basics and discussion surrounding the Ehrenfest Force **F**(**r**), stress tensor **σ**(**r**) and the bond-path framework set $\mathsf{B} = \{\boldsymbol{p},\boldsymbol{q},\boldsymbol{r}\}$.

2. Supplementary Materials S2. Computational protocol and numerical evaluation of the Ehrenfest force **F**(**r**) partitioning.

3. Supplementary Materials S3. Poincaré-Hopf solution sets and the results for QTAIM and Ehrenfest Force **F**(**r**) partitioning schemes and plots comparing *BCP* and *NNA* properties with charged Li clusters.

4. Supplementary Materials S4. The bond-path framework sets for the QTAIM and Ehrenfest partitioning molecular graphs of the Li_m (m = 2-5) clusters.

5. Supplementary Materials S5. The variation of ellipticity ε profile with distance along Li-*BCP*-*NNA*-*BCP*-Li separation for the Li_m (m = 2-5) clusters.

6. Supplementary Materials S6. The variation of ellipticity ε, ε_σ, $\varepsilon_{\sigma H}$, ε_{FB} with distance along the Li-Li separation for the Ehrenfest partitioning for Li_m (m = 2-5) clusters.

7. Supplementary Materials S8. The QTAIM and Ehrenfest Force **F**(**r**) partitioning measures for compressed and stretched molecular graphs of the Li_2 cluster.

1. Supplementary Materials S1.

(i) The QTAIM BCP and bond-path properties; BPL, the helicity lengths H, H and the bond-path framework set B*

QTAIM that utilizes higher derivatives of $\rho(\mathbf{r_b})$ in effect, acting as a 'magnifying lens' on the $\rho(\mathbf{r_b})$ derived properties of the wave-function to identify critical points in the total electronic charge density distribution $\rho(\mathbf{r})$ by analyzing the gradient vector field $\nabla\rho(\mathbf{r})$. These critical points can further be divided into four types of topologically stable critical points according to the set of ordered eigenvalues $\lambda_1 < \lambda_2 < \lambda_3$, with corresponding eigenvectors $\underline{\mathbf{e}}_1$, $\underline{\mathbf{e}}_2$, $\underline{\mathbf{e}}_3$ of the Hessian matrix. The Hessian of the total electronic charge density $\rho(\mathbf{r})$ is defined as the matrix of partial second derivatives with respect to the spatial coordinates. These critical points are labeled using the notation (R, ω) where R is the rank of the Hessian matrix, the number of distinct non-zero eigenvalues and ω is the signature (the algebraic sum of the signs of the eigenvalues); the (3, -3) [nuclear critical point (*NCP*), a local maximum generally corresponding to a nuclear location], (3, -1) and (3, 1) [saddle points, called bond critical points (*BCP*) and ring critical points (*RCP*), respectively] and (3, 3) [the cage critical points (*CCP*)]. In the limit that the forces on the nuclei become vanishingly small, an atomic interaction line [Bader, *J. Phys. Chem. A*, 1998, **102**, 7314–7323] becomes a bond-path, although not necessarily a chemical bond [Bader. *J. Phys. Chem. A*. 2009, **113**, 10391-10396] with the complete set of critical points and the bond-paths of a molecule being referred to as the molecular graph.

The total local energy density $H(\mathbf{r}_b)$ [S. Jenkins, *Phys. Chem. Chem. Phys.*, 2014, **16**, 7115–7126.], [E. Kraka, *J. Mol. Struct. THEOCHEM*, 1992, **255**, 189–206.]

$$H(\mathbf{r}_b) = G(\mathbf{r}_b) + V(\mathbf{r}_b), \qquad \textbf{(1)}$$

where $G(\mathbf{r}_b)$ and $V(\mathbf{r}_b)$ in equation **(1)** are the local kinetic and potential energy densities at a *BCP*, defines a degree of covalent character: A negative value for $H(\mathbf{r}_b) < 0$ for the closed-shell interaction, a value of the Laplacian $\nabla^2\rho(\mathbf{r}_b) > 0$, indicates a *BCP* with a degree of covalent character and conversely a positive value of $H(\mathbf{r}_b) > 0$ reveals a lack of covalent character for the closed-shell *BCP*. A shared-shell *BCP* always possesses both Laplacian $\nabla^2\rho(\mathbf{r}_b) < 0$ and $H(\mathbf{r}_b) < 0$.

The bond-path length (BPL) is defined as the length of the path of the $\underline{\mathbf{e}}_3$ eigenvector of λ_3 eigenvalue, defined at the *BCP*, of the Hessian of the total charge density $\rho(\mathbf{r})$ that follows the maximum in $\rho(\mathbf{r})$. The bond-path curvature separating two bonded nuclei is defined as the dimensionless ratio:

$$(\text{BPL} - \text{GBL})/\text{GBL}, \qquad \textbf{(2)}$$

Where BPL is as the associated bond-path length and the geometric bond length GBL is the inter-nuclear separation. The BPL often exceeds the GBL particularly for weak or strained bonds and unusual bonding environments. [*J. Phys. Condens. Matter*, 2000, **12**, 10325.] Earlier, one of the current authors hypothesized that a bond-path may possess 1-D, 2-D or a 3-D topology. [*Chem. Phys. Lett.*, 2000, **317**, 97–102.] Bond-paths possessing zero and non-zero values of the bond-path curvature defined by equation **(11)** can be considered to possess 1-D and 2-D topologies respectively. For some systems subject to an applied torsion θ however, the torsional *BCP* may display negligible variation in the bond-path curvature defined by equation **(11)**. Therefore, a new measure that is more appropriate for bonds with negligible values of the curvature is required. We choose this quantity to be the length traced out in 3-D by the path swept by the tips of the scaled $\underline{\mathbf{e}}_2$ eigenvectors of the λ_2 eigenvalue, the scaling factor could be the ellipticity ε.

With n scaled eigenvector $\underline{\mathbf{e}}_2$ tip path points $q_i = r_i + \varepsilon_i \underline{\mathbf{e}}_{2,i}$ on the path q where ε_i = ellipticity at the i^{th} bond-path point r_i on the bond-path r. It should be noted that the bond-path is associated with the λ_3 eigenvalues of the $\underline{\mathbf{e}}_3$ eigenvector does not take into account differences in the λ_1 and λ_2 eigenvalues of the $\underline{\mathbf{e}}_1$ and $\underline{\mathbf{e}}_2$ eigenvectors. Analogously, for the $\underline{\mathbf{e}}_1$ tip path points we have $p_i = r_i + \varepsilon_i \underline{\mathbf{e}}_{1,i}$ on the path p where ε_i = ellipticity at the i^{th} bond-path point r_i on the bond-path r.

We will refer to the new QTAIM interpretation of the chemical bond as the *bond-path framework set* that will be denoted by B, where $\mathsf{B} = \{p, q, r\}$. This effectively means that in the most general case a bond is comprised of three 'linkages'; p, q and r associated with the $\underline{\mathbf{e}}_1$, $\underline{\mathbf{e}}_2$ and $\underline{\mathbf{e}}_3$ eigenvectors, respectively.

The p and q parameters define helicity length H and H^*, see **Scheme S1**:

$$\mathsf{H} = \sum_{i=1}^{n-1} |q_{i+1} - q_i| \qquad \textbf{(3a)}$$

$$\mathsf{H}^* = \sum_{i=1}^{n-1} |p_{i+1} - p_i| \qquad \textbf{(3b)}$$

The *helicity* length H or H^* refers to the fact that the tips of the scaled $\underline{\mathbf{e}}_2$ or $\underline{\mathbf{e}}_1$ eigenvectors will rotate along the extent of the bond-path, defined by the $\underline{\mathbf{e}}_3$ eigenvector, between the two bonded nuclei that the bond-path connects.

In the limit of vanishing ellipticity ε = 0, *for all* steps i along the bond-path, one has H = BPL and H > BPL otherwise. For a pure BLA coordinate motion comprising bond-paths with negligible curvature the $\{\underline{\mathbf{e}}_1, \underline{\mathbf{e}}_2, \underline{\mathbf{e}}_3\}$ bond-path framework does not undergo a torsional distortion therefore there is no relative change of the λ_1 and

λ_2 eigenvalues for all values of the scaling factor ε_i. Additionally, because H and H* are defined by the distances swept out by the $\underline{\mathbf{e}}_2$ tip path points, $q_i = r_i + \varepsilon_i \underline{\mathbf{e}}_{2,i}$ and $p_i = r_i + \varepsilon_i \underline{\mathbf{e}}_{1,i}$ respectively, one has H = H* provided that identical scaling factor ε_i is used in equations **(3a)** and **(3b)**.

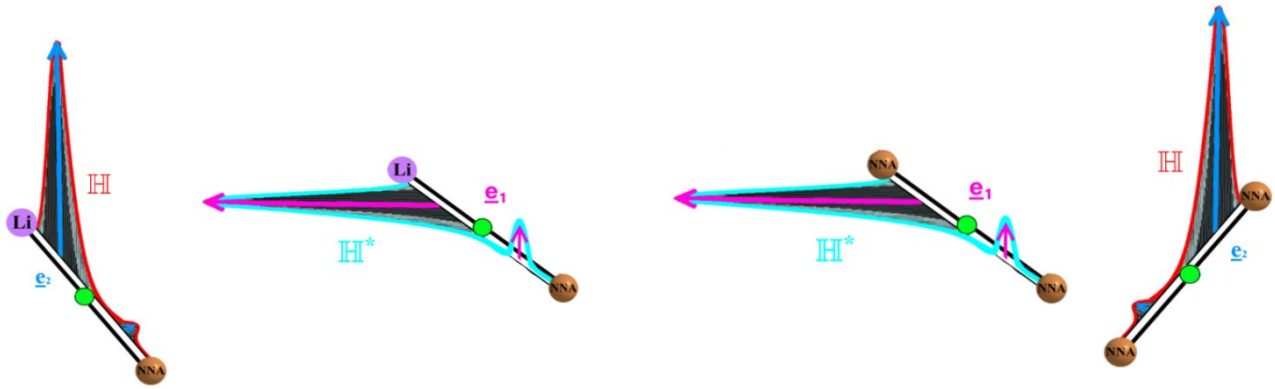

(a) **(b)** **(c)** **(d)**

Scheme S1. The red line represents the helical path swept out by the tips of the scaled $\underline{\mathbf{e}}_2$ eigenvectors that we refer to as the helicity length H that is defined by equation **(3a)**. The two blue arrows represented $\underline{\mathbf{e}}_2$ eigenvectors scaled by the ellipticity ε where the vertical scales are exaggerated for visualization purposes. The green sphere indicates the position of the torsional Li-*NNA*, *NNA-NNA BCP*s. The path representing the helicity length H* is not shown for clarity, is constructed from the tips of the scaled $\underline{\mathbf{e}}_1$ eigenvectors that are mutually perpendicular to the $\underline{\mathbf{e}}_2$ and $\underline{\mathbf{e}}_3$ eigenvectors, defined by equation **(3b)**.

A bond within QTAIM is defined as being the bond-path traversed by along $\underline{\mathbf{e}}_3$ eigenvector of the λ_3 eigenvector from the bond-path, but, as a consequence of equation **(3)**, this definition should be expanded. The new definition of a bond should consider the bond-path to comprise the two paths swept out by the $\underline{\mathbf{e}}_2$ and $\underline{\mathbf{e}}_1$ eigenvectors that form the helicity length H and H*, respectively.

*(ii) Ehrenfest Force **F(r)**, see also the main text*

Consequently **F**(**r**) can be proposed in terms of the molecular Coulomb potential integral equation or in terms of the divergence of the quantum stress tensor. The latter form of **F**(**r**) allows us to map onto a surface integral **S**(**r**) using the Gauss's theorem as an integration of the force density, over the basin of an atom Ω:

$$F(\Omega) = -N \oint_{\Omega} dS(r,\Omega) \cdot \sigma(r) \qquad \textbf{(1)}$$

Thus **σ**(**r**) can be used to determine the force exerted on each element of the atomic surface, $S(\mathbf{r},\Omega)$, and its product with an element of the surface gives the force acting on this region. [*Faraday Discuss,* 2006, **135**, 79–95.], [*Chem. - Eur. J.*, 2012, **18**, 4982–4993.] Consider a tiny cube of fluid flowing in 3-D space the stress Π(*x*,

y, *z*, *t*), a rank-3 tensor field, has nine components [Wyatt, R. E. Quantum Dynamics with Trajectories. *Interdiscip. Appl. Math.* xxii,405 (2006).] of these the three diagonal components Π_{xx}, Π_{yy}, and Π_{zz} correspond to normal stress. A negative value for these normal components signifies a compression of the cube, conversely a positive value refers to pulling or tension, where more negative/positive values correspond to increased compression/tension of the cube. Diagonalization of the stress tensor, $\sigma(\mathbf{r})$, returns the principal electronic stresses Π_{xx}, Π_{yy}, and Π_{zz} that are realized as the stress tensor eigenvalues $\lambda_{1\sigma}$, $\lambda_{2\sigma}$, $\lambda_{3\sigma}$, with corresponding eigenvectors $\underline{\mathbf{e}}_{1\sigma}$, $\underline{\mathbf{e}}_{2\sigma}$, $\underline{\mathbf{e}}_{3\sigma}$ are calculated within the QTAIM partitioning.

As a comparison with the examination of the gradient of the electron density in the QTAIM theory, a complementary scheme can be proposed from the investigation of the primitive amount of the Ehrenfest Force, the Ehrenfest potential, $V^{\mathrm{F}}(\mathbf{r})$, using the definition:

$$F(r) = -\nabla V^{F}(r) \qquad \textbf{(2)}$$

Alongside the condition that the potential energy of interaction of an electron at an infinite distance from a molecule is zero:

$$\lim_{|r| \to \infty} \mathrm{V}^{F}(r) = 0 \qquad \textbf{(3)}$$

With this definition, $V^{\mathbf{F}}(\mathbf{r})$ is closely related to the average potential defined by Slater. [*Phys. Rev.*, 1951, **81**, 385–390.], [*Int. J. Quantum Chem.*, 1997, **62**, 47–53.] In this analogy we can follow the trajectories of $\mathbf{F}(\mathbf{r})$ that terminate at points where $\mathbf{F}(\mathbf{r}) = 0$. One can then calculate and observe inter atomic Ehrenfest Force surfaces which satisfy the zero-flux condition $\mathbf{F}(\mathbf{r})\cdot\mathbf{n}(\mathbf{r}) = 0$. The Ehrenfest Hessian may then also be defined as $\nabla\nabla\cdot\boldsymbol{\sigma}(\mathbf{r})$.

The *BCP* can be characterized similarly to the critical points (CP) of the electron density distribution in QTAIM as long as at the Ehrenfest *BCP*s all the force applied on an electron are balanced [*J. Chem. Phys.*, 2009, **130**, 154104.] ($\mathbf{F}(r) = 0$) , *i.e.* with the notation (3, -1), according to the eigenstructure (eigenvalues/eigenvectors) of the Ehrenfest Hessian.

The advantage of using the Ehrenfest partitioning is to gain physically meaning for a capping surface at a threshold value of $V^{\mathbf{F}}(\mathbf{r})$, that it is the outer boundary of molecule. We can use, for example, the ionization potential V_{I} to define the molecular boundary using: [*Phys. Rev. A*, 1991, **44**, 7071–7083.]

$$V^{F}(r) = -V_{I} \qquad \textbf{(4)}$$

Ionization energy E_{I}, or ionization potential V_{I}, is the minimum amount of necessary energy to remove an electron from the neutral atom that can be determined from experiment. By contrast, within QTAIM the

somewhat arbitrary conventional definition of the molecular boundary uses a threshold of 0.001 a.u. for the electron density.

2. Supplementary Materials S2. Computational protocol and numerical evaluation of the Ehrenfest force **F**(**r**) partitioning

The inherent difficulties of the computation of the Ehrenfest force **F**(**r**) were examined during a previous investigation by some of the current authors, [*Phys. Chem. Chem. Phys.*, 2013, **15**, 17823–17836.] attributing the spurious artifacts to the diffuse GTOs used in basis sets. Research has been undertaken in accurately computing quantum stress tensor properties using Gaussian basis sets. In the work by Tachibana *et al*., [*J. Mol. Struct. THEOCHEM*, 2010, **951**, 49–59.] they studied the effect of the basis sets expansion on the electronic stress tensor calculations, compared with the exact wave function for the ion H+ 2, showing that the calculations for *cc*-pV5Z and *cc*-pV6Z basis sets are in close agreement with the *spindle* form of the exact wave function. In addition, other authors[*J. Chem. Phys.*, 2012, **137**, 134101.] showed the effect of the basis sets on the stress tensor, calculating the profiles of the magnitude of the attractive **F**(**r**) for the H and H_2 ground states. In this case, the expanded basis set aug-*cc*-pV5Z provided the best agreement with the exact computation of **F**(**r**). It was suggested in 2007 by Hernández-Trujillo and co-workers that spurious artifacts are pushed into the bonding regions upon close-approach of the nuclei [*Faraday Discuss.*, 2007, **135**, 79–95.] in the **F**(**r**) calculations if GTOs with s and p functions with exponents of order of 10^5 and 10^3 were used. This can be contrasted with conventional basis sets such as pV6Z which have exponent values of order 10^3 and 10^1 respectively. Following that suggestion we decided to use the extended relativistic Atomic Natural Orbital (ANO-RCC) GTO basis sets developed by Ross and collaborators. [*Theor. Chim. Acta*, 1990, **77**, 291–306.], [*Theor. Chem. Acc.*, 2004, **111**, 345–351.], [*J. Phys. Chem. A*, 2005, **109**, 6575–6579.] These basis sets were constructed by averaging over several atomic states, positive and negative ions and atoms in an external electric field, with the key feature that they are highly focused at the nuclei.

(i) Computational protocol

Previously, as a starting point, some of the current authors, decided that the standard *cc*-pV5Z and *cc*-pV6Z basis sets cannot be modified by removing the same number of exponents in each GTO. [*Phys. Chem. Chem. Phys.*, 2013, **15**, 17823–17836.] This was because in these basis sets the same kind of Gaussian functions have different numbers of exponents, thus an uneven modification of the standard basis sets causes a loss of the functional nature of the basis set. The ANO-RCC basis sets, however, have the same number of exponents in each GTO, allowing us to remove the same number of exponents from each function in the GTO. For each atom the basis sets were rewritten into the form of the standard basis sets (*cc*-pVXZ(X = D,T,Q)), then only exponents in a specific range for each function were kept and the others removed. This yielded a new kind of

modified ANO RCC basis set where the highly focused functions prevail over diffuse functions. Thus each atom has an *engineered* ANO-RCC basis set: values for the preserved exponents in each basis set can be found in our previous contribution. [*Phys. Chem. Chem. Phys.*, 2013, **15**, 17823–17836.] These values were determined by calculation of the **F**(**r**) trajectories for each modified basis set with different ranges of exponents until a well-behaved set of **F**(**r**) (free of spurious features) was obtained.

(ii) Numerical evaluation of the Ehrenfest force F(r) Partitioning Scheme

A convenient start point is the simple system, H_2, which is a highly symmetrical molecule, with an Ehrenfest *BCP* halfway between the two hydrogen nuclei. Fig. 1 shows the Ehrenfest force trajectory calculation for the H_2 molecule. In Fig. 1(a) and (b) the aug-*cc*-pVQZ basis set and the non-modified ANO-RCC basis sets were respectively used. These basis sets contain diffuse functions and despite the fact that in the ANO-RCC the functions are more localized at the nuclei than in the aug-*cc*-pVQZ, the appearance of spurious features evidenced a strong dependence of the computation of the **F**(**r**) on the presence of diffuse functions in the basis sets. The *cc*-pVQZ basis set contains 10 GTOs (4s,3p,2d,1f) while ANO-RCC contains 16 GTOs (8s,4p,3d,1f) and although the shape of the **F**(**r**) trajectories is mostly the same, the location of the spurious features changes by 1 a.u., further away from the nuclei. The original aug-*cc*-pVQZ was not modified and therefore not shown (for details refer to subsection (i)), Fig. 1(c) shows the modified ANO-RCC basis (for the values in the preserved exponents [*Phys. Chem. Chem. Phys.*, 2013, **15**, 17823–17836.]). The plot does not contain any spurious surfaces and a monotonic behaviour of the **F**(**r**) is apparent. Considering that higher order derivatives used in the computation of the **F**(**r**) may act to magnify errors in the **F**(**r**) calculation, to ensure a correct calculation, the researcher should be particularly careful with the critical point properties calculated from the optimized geometries.

3. Supplementary Materials S3. Poincaré-Hopf solution sets of the QTAIM and Ehrenfest Force **F**(**r**) partitioning schemes and plots comparing *BCP* and *NNA* properties with charged Li clusters.

Table S3(i). The solution sets of the Poincaré-Hopf relation for the topology results from the QTAIM partitioning scheme using the ANO-RCC basis set, for each value of m the Li_m neutral. The topological complexity $\sum_{abrc}$ represents the sum the *BCP*s (***b***), *RCP*s (***r***) and *CCP*s (***c***) and quantum topology is denoted by D_{QT}.

Li_m (m = 2-5)	*Multiplicity*	*a*	*b*	*r*	*c*	$\sum_{abrc}$	D_{QT}
Li_2	1	1	2	0	0	3	1
Li_3	2	1	3	0	0	4	1
Li_4 (1)	1	2	7	2	0	11	2
Li_4 (2)	1	2	5	0	0	7	1
Li_5 (1)	2	3	0	3	0	16	2
Li_5 (2)	2	2	8	2	0	12	2

Table S3(ii). The Poincaré-Hopf topologies from Ehrenfest Force **F**(**r**) partitioning scheme, see the caption of **Table S3(i)** for further details.

Li_m (m = 2-5)	*m*	*a*	*b*	*r*	*c*	$\sum_{abrc}$	D_{QT}
Li_2	2	0	1	0	0	1	1
Li_3	3	0	2	0	0	2	1
Li_4 (1)	4	0	5	2	0	7	2
Li_4 (2)	4	0	4	1	0	5	2
Li_5 (1)[a]	5	0	7	3	0	10	2
Li_5 (2)	5	0	6	2	0	8	2

[a] modified ANO-RCC basis set.

Table S3(iii). The QTAIM partitioning scheme *BCP* and *NNA* measures where the subscripts '$_b$' and '$_a$' refer to the *BCP* and *NNA* respectively, for the molecular graphs of the Li_m (m = 2-5) clusters. The Li-*NNA BCP, NNA-NNA BCP* and *NNA-BCP* distance refer to separations, Laplacian $\nabla^2\rho(\mathbf{r}_a)$ and $\rho(\mathbf{r}_a)$ of the *NNA*, the Li-*NNA BCP*, Laplacian $\nabla^2\rho(\mathbf{r}_b)$, $\rho(\mathbf{r}_b)$, total local energy density $H(\mathbf{r}_b)$, metallicity $\xi(\mathbf{r}_b)$, ellipticity ε are presented, atomic units are used, refer to the left panels of **Figures 1** for the corresponding molecular graphs.

Li_m^q	*BCP*	Li-*NNA*, *NNA*-*NNA*	*NNA*-*BCP*	$\rho(\mathbf{r}_a)$	$\nabla^2\rho(\mathbf{r}_a)$	$\rho(\mathbf{r}_b)$	$\nabla^2\rho(\mathbf{r}_b)$	$H(\mathbf{r}_b)$	$\xi(\mathbf{r}_b)$	ε
Li_2	Li1-*NNA*3	2.5518	0.7273	0.0142	-0.0134	0.0135	0.0039	-0.0024	3.4523	0.0000
	Li2-*NNA*3	2.5518	0.7273	0.0142	-0.0134	0.0135	0.0039	-0.0024	3.4523	0.0000
Li_3	Li1-*NNA*4	2.6233	0.7554	0.0134	-0.0080	0.0128	0.0054	-0.0019	2.3628	6.5936
	Li2-*NNA*4	3.6442	1.7056	0.0134	-0.0080	0.0123	0.0058	-0.0018	2.1339	0.9832
	Li3-*NNA*4	3.6423	1.7036	0.0134	-0.0080	0.0123	0.0058	-0.0018	2.1340	0.9838
Li_4 (1)	Li1-*NNA*5	2.7088	0.8841	0.0143	-0.0099	0.0135	0.0058	-0.0019	2.3284	0.5630
	Li2-*NNA*5	3.4458	1.5870	0.0143	-0.0099	0.0122	0.0063	-0.0017	1.9308	0.9548
	Li2-*NNA*6	3.4507	1.5925	0.0143	-0.0100	0.0123	0.0064	-0.0017	1.9144	0.9450
	Li3-*NNA*5	3.4490	1.5901	0.0143	-0.0099	0.0122	0.0063	-0.0017	1.9272	0.9561
	Li3-*NNA*6	3.4360	1.5779	0.0143	-0.0100	0.0123	0.0064	-0.0018	1.9278	0.9395
	Li4-*NNA*6	2.7045	0.8813	0.0143	-0.0100	0.0135	0.0058	-0.0019	2.3148	0.5646
	*NNA*5-*NNA*6	4.8509	2.4224	0.0143	-0.0099	0.0110	-0.0033	-0.0023	-3.3074	0.5696
			2.4285	0.0143	-0.0100					
Li_4 (2)	Li1-*NNA*5	2.5563	0.6992	0.0130	-0.0117	0.0125	0.0028	-0.0022	4.4135	0.0134
	Li2-*NNA*5	2.7107	0.8338	0.0130	-0.0117	0.0123	0.0020	-0.0022	6.1524	0.0248
	Li2-*NNA*6	4.8483	2.9599	0.0152	-0.0126	0.0092	0.0070	-0.0009	1.3027	0.2742
	Li3-*NNA*6	2.6114	0.7999	0.0152	-0.0126	0.0143	0.0055	-0.0024	2.6032	0.4763
	Li4-*NNA*6	2.6131	0.8018	0.0152	-0.0126	0.0143	0.0055	-0.0024	2.5872	0.4718
Li_5 (1)	Li1-*NNA*6	3.7699	1.8774	0.0137	-0.0095	0.0111	0.0065	-0.0014	1.7204	1.0697
	Li1-*NNA*7	3.7805	1.8871	0.0137	-0.0095	0.0111	0.0065	-0.0014	1.7186	1.0754
	Li2-*NNA*6	2.6533	0.7981	0.0137	-0.0095	0.0131	0.0042	-0.0020	3.1155	0.7242
	Li3-*NNA*7	2.6527	0.7967	0.0137	-0.0095	0.0131	0.0042	-0.0020	3.1371	0.7247
	Li4-*NNA*7	3.3202	1.4655	0.0137	-0.0095	0.0120	0.0064	-0.0016	1.8809	0.7622
	Li4-*NNA*8	2.8890	0.9577	0.0109	-0.0076	0.0103	0.0028	-0.0017	3.6314	1.5040
	Li5-*NNA*6	3.3228	1.4685	0.0137	-0.0095	0.0120	0.0064	-0.0016	1.8743	0.7618
	Li5-*NNA*8	2.8873	0.9557	0.0109	-0.0076	0.0103	0.0028	-0.0017	3.6486	1.5073
	*NNA*6-*NNA*8	4.7190	2.9402	0.0137	-0.0095	0.0099	-0.0036	-0.0018	-2.7760	1.1691
			1.7613	0.0109	-0.0076					
	*NNA*7-*NNA*8	4.7188	2.9373	0.0137	-0.0095	0.0099	-0.0036	-0.0018	-2.7767	1.1682
			1.7639	0.0109	-0.0076					
Li_5 (2)	Li1-*NNA*6	2.9977	1.1062	0.0135	-0.0076	0.0127	0.0060	-0.0017	2.1088	0.9636
	Li2-*NNA*6	4.6291	2.5994	0.0135	-0.0076	0.0106	0.0073	-0.0013	1.4630	0.9844
	Li2-*NNA*7	3.4908	1.6208	0.0142	-0.0100	0.0120	0.0069	-0.0016	1.7273	0.5472
	Li3-*NNA*6	4.6309	2.6010	0.0135	-0.0076	0.0106	0.0073	-0.0013	1.4634	0.9841
	Li3-*NNA*7	3.4907	1.6207	0.0142	-0.0100	0.0120	0.0069	-0.0016	1.7274	0.5471
	Li4-*NNA*7	2.6041	0.7712	0.0142	-0.0100	0.0135	0.0050	-0.0020	2.6971	0.6138
	Li5-*NNA*6	2.9975	1.1060	0.0135	-0.0076	0.0127	0.0060	-0.0017	2.1089	0.9635

*NNA*6-*NNA*7	5.8543	3.0748	0.0135	-0.0076	0.0096	-0.0016	-0.0016	-6.0600	0.6758
		2.7795	0.0142	-0.0100					

Table S3(iv). The results for Ehrenfest Force **F**(**r**) partitioning molecular graph of the Li_m (m = 2-5) clusters, where the bonded Li *NCP*- Li *NCP* separations, $\nabla^2\rho(\mathbf{r_{Fb}})$, $\rho(\mathbf{r_{Fb}})$, $H(\mathbf{r_{Fb}})$, $\xi(\mathbf{r_{Fb}})$, two choices of the Ehrenfest Force **F**(**r**) ellipticity $\varepsilon_{FA} = (|\lambda_{1F}|/|\lambda_{2F}|) - 1$ and Ehrenfest ellipticity $\varepsilon_{FB} = (|\lambda_{2F}|/|\lambda_{1F}|) - 1$ are presented, refer to the main text and the right panels of **Figures 1** for the corresponding molecular graphs. The QTAIM ellipticity $\varepsilon = (|\lambda_1|/|\lambda_2|) - 1$, stress tensor ellipticities $\varepsilon_\sigma = (|\lambda_{2\sigma}|/|\lambda_{1\sigma}|) - 1$ and $\varepsilon_{\sigma H} = (|\lambda_{1\sigma}|/|\lambda_{2\sigma}|) - 1$ are calculated on the Ehrenfest Force **F**(**r**) molecular graph, where the subscript "$_H$" refers to the ordering of the eigenvalues that corresponds to the Hessian.

Li_m (m = 2-5) *BCP*	Li-Li	$\rho(\mathbf{r_{Fb}})$	$\nabla^2\rho(\mathbf{r_{Fb}})$	$H(\mathbf{r_{Fb}})$	$\xi(\mathbf{r_{Fb}})$	ε	ε_σ	$\varepsilon_{\sigma H}$	ε_{FA}	ε_{FB}
Li_2	Li1-Li2	5.1035	0.0142	-0.0134	-0.0035	-1.0635	0.0000	-0.2279	0.2951	0.0000	0.0000
Li_3	Li1-Li2	5.1997	0.0124	-0.0089	-0.0028	-1.3930	0.9766	-0.1467	0.1720	1.2190	0.5493
	Li1-Li3	5.1995	0.0124	-0.0089	-0.0028	-1.3930	0.9677	-0.1462	0.1712	1.2355	0.5527
Li_4 (1)	Li1-Li2	5.6840	0.0130	-0.0092	-0.0025	-1.4169	0.6438	-0.2713	0.3723	0.5437	0.3516
	Li1-Li3	5.6851	0.0130	-0.0092	-0.0025	-1.4176	0.5927	-0.2574	0.3466	0.4518	0.3112
	Li2-Li3	4.8650	0.0110	-0.0033	-0.0023	-3.3074	0.4643	-0.0262	0.0270	0.0103	0.0102
	Li2-Li4	5.6783	0.0130	-0.0092	-0.0025	-1.4136	0.5969	-0.2582	0.3481	0.4481	0.3095
	Li3-Li4	5.6700	0.0130	-0.0093	-0.0025	-1.4089	0.6374	-0.2691	0.3683	0.4503	0.3507
Li_4 (2)	Li1-Li2	5.2669	0.0130	-0.0117	-0.0031	-1.1072	0.0044	-0.0044	0.0044	0.0174	0.0171
	Li2-Li3	5.9296	0.0096	-0.0053	-0.0016	-1.8311	0.8450	-0.3042	0.4373	0.9147	0.4777
	Li2-Li4	5.9433	0.0096	-0.0053	-0.0016	-1.8346	0.8886	-0.3131	0.4558	0.8723	0.4660
	Li3-Li4	5.1235	0.0147	-0.0126	-0.0035	-1.1715	0.0747	-0.0468	0.0490	0.0597	0.0563
Li_5 (1)[a]	Li1-Li2	5.6115	0.0115	-0.0078	-0.0022	-1.4741	0.3982	-0.1922	0.2380	0.0232	0.0227
	Li1-Li3	5.6170	0.0115	-0.0078	-0.0022	-1.4780	0.3973	-0.1923	0.2380	0.1288	0.1140
	Li1-Li4	5.3906	0.0102	-0.0043	-0.0019	-2.3773	0.9481	-0.1681	0.2020	0.1982	0.4512
	Li1-Li5	5.3846	0.0103	-0.0043	-0.0019	-2.3710	0.9387	-0.1678	0.2016	1.0411	0.5101
	Li3-Li4	5.5930	0.0125	-0.0091	-0.0025	-1.3653	0.3881	-0.2040	0.2563	1.0490	0.5120
	Li2-Li5	5.5934	0.0125	-0.0091	-0.0025	-1.3656	0.3914	-0.2053	0.2583	0.7806	0.4384
	Li4-Li5	5.7536	0.0108	-0.0080	-0.0023	-1.3545	0.3231	-0.1168	0.1323	0.1244	0.1106
Li_5 (2)	Li1-Li3	5.3715	0.0110	-0.0066	-0.0022	-1.6567	0.1909	-0.0382	0.0380	1.1933	0.5440
	Li2-Li3	5.1069	0.0100	-0.0023	-0.0018	-4.3624	0.4219	-0.0830	0.0904	0.9728	0.4931
	Li2-Li4	5.5654	0.0127	-0.0090	-0.0025	-1.4017	0.4452	-0.1743	0.2112	0.5451	0.3529
	Li3-Li4	5.5654	0.0127	-0.0090	-0.0025	-1.4017	0.4452	-0.1743	0.2111	0.5553	0.3570
	Li1-Li5	5.4890	0.0122	-0.0081	-0.0024	-1.5067	0.1856	-0.0561	0.0593	1.5223	0.6035
	Li2-Li5	5.3715	0.0110	-0.0066	-0.0022	-1.6568	0.1909	-0.0383	0.0399	1.2018	0.5458

[a] modified ANO-RCC basis set.

Table S3(v). The eigenvector following path lengths (H,H′), (H_σ,H_σ′), ($H_{\sigma H}$,$H_{\sigma H}$′), (H_{FA},H_{FA}′) and (H_{FB},H_{FB}′) obtained by projecting eigenvectors onto the Ehrenfest Force **F**(**r**) molecular graph. Note, $\varepsilon_{FA} = (|\lambda_{1F}|/|\lambda_{2F}|) - 1$ and $\varepsilon_{FB} = (|\lambda_{2F}|/|\lambda_{1F}|) - 1$.

Li_m	*BCP*	(H,H′)		(H_σ,H_σ′)		($H_{\sigma H}$,$H_{\sigma H}$′)		(H_{FA},H_{FA}′)		(H_{FB},H_{FB}′)	
Li_2											
	Li1-Li2	(5.104, 5.104)	(5.104, 5.104)	(5.573, 5.573)	(6.570, 6.570)	(7.301, 7.301)	(9.110, 9.110)	(5.104, 5.104)	(5.104, 5.104)	(5.104, 5.104)	(5.104, 5.104)
Li_3											
	Li1-Li2	(5603, 5597)	(5601, 5598)	(9.922, 10.02)	(9.978, 10.01)	(10.25, 10.14)	(10.26, 10.21)	(10.28, 10.40)	(10.30, 10.37)	(9.983, 9.925)	(9.969, 9.939)
	Li1-Li3	(10061, 10061)	(10063, 10065)	(9.919, 10.02)	(10.00, 9.978)	(10.25, 10.14)	(10.21, 10.26)	(10.41, 10.29)	(10.32, 10.39)	(9.928, 9.984)	(9.939, 9.972)
Li_4 (1)											
	Li1-Li2	(10.93, 10.93)	(10.98, 10.89)	(11.27, 11.89)	(12.08, 12.14)	(15.32, 14.41)	(15.40, 15.32)	(10.87, 10.99)	(10.94, 10.92)	(10.86, 10.77)	(10.81, 10.83)
	Li2-Li3	(9.458, 9.458)	(9.459, 9.458)	(9.879, 9.880)	(10.34, 10.34)	(11.42, 11.42)	(11.86, 11.86)	(9.207, 9.207)	(9.207, 9.207)	(9.205, 9.205)	(9.205, 9.205)
	Li2-Li4	(10.90, 10.90)	(10.95, 10.86)	(11.87, 11.27)	(12.12, 12.07)	(14.40, 15.29)	(15.29, 15.35)	(10.82, 10.92)	(10.86, 10.88)	(10.83, 10.76)	(10.80, 10.78)
Li_4 (2)											
	Li1-Li2	(9.953, 9.953)	(9.953, 9.953)	(10.84, 10.86)	(11.30, 11.30)	(14.55, 14.53)	(14.90, 14.90)	(9.953, 9.953)	(9.953, 9.953)	(9.953, 9.953)	(9.953, 9.953)
	Li2-Li3	(11.50, 11.50)	(11.50, 11.50)	(11.98, 12.00)	(12.61, 12.62)	(16.26, 16.22)	(16.83, 16.80)	(11.54, 11.54)	(11.53, 11.56)	(11.30, 11.30)	(11.31, 11.29)
	Li3-Li4	(9.687, 9.687)	(9.688, 9.686)	(10.59, 10.59)	(11.03, 11.06)	(13.77, 13.77)	(14.16, 14.13)	(9.683, 9.684)	(9.684, 9.684)	(9.684, 9.683)	(9.684, 9.684)
Li_5 (1)											
	Li1-Li2	(10.67, 10.67)	(10.65, 10.68)	(11.48, 11.38)	(11.95, 11.98)	(14.50, 14.64)	(15.08, 15.04)	(10.62, 10.62)	(10.62, 10.62)	(10.61, 10.62)	(10.61, 10.62)
	Li1-Li5	(10.60, 10.60)	(10.57, 10.64)	(10.97, 10.92)	(12.60, 12.57)	(14.02, 14.07)	(16.60, 16.65)	(10.81, 10.82)	(10.77, 10.86)	(10.32, 10.31)	(10.34, 10.29)
	Li2-Li5	(10.63, 10.63)	(10.62, 10.64)	(11.49, 11.46)	(11.98, 12.04)	(15.33, 15.39)	(15.84, 15.77)	(10.90, 10.89)	(10.86, 10.93)	(10.66, 10.67)	(10.67, 10.72)
	Li4-Li5	(10.93, 10.93)	(10.95, 10.92)	(11.04, 12.04)	(13.01, 13.02)	(16.13, 14.64)	(17.24, 17.23)	(10.89, 10.89)	(10.90, 10.89)	(10.89, 10.89)	(10.89, 10.89)
Li_5 (2)											
	Li1-Li3	(10.21, 10.21)	(10.23, 10.19)	(10.96, 10.95)	(11.50, 11.47)	(14.73, 14.75)	(15.19, 15.24)	(10.54, 10.83)	(10.66, 10.70)	(10.36, 10.21)	(10.29, 10.28)
	Li2-Li3	(9.797, 9.797)	(9.768, 9.826)	(10.48, 10.48)	(11.05, 11.11)	(14.09, 14.09)	(14.76, 14.69)	(9.879, 10.04)	(9.955, 9.956)	(9.793, 9.702)	(9.747, 9.747)
	Li1-Li5	(10.42, 10.42)	(10.44, 10.40)	(11.23, 11.23)	(11.76, 11.73)	(15.16, 15.16)	(15.56, 15.61)	(11.34, 11.03)	(11.18, 11.18)	(10.46, 10.60)	(10.53, 10.53)
	Li2-Li5	(10.21, 10.21)	(10.23, 10.19)	(10.95, 10.96)	(11.47, 11.50)	(14.75, 14.73)	(15.24, 15.19)	(10.84, 10.55)	(10.68, 10.71)	(10.21, 10.36)	(10.29, 10.28)

Table S3(vi). The QTAIM partitioning scheme *BCP* and *NNA* measures where the subscripts '$_{\mathbf{b}}$' and '$_{\mathbf{a}}$' refer to the *BCP* and *NNA* respectively, for the molecular graphs of the Li_m^q (m = 2-5, q = ±1) clusters. The Li-*NNA BCP, NNA-NNA BCP* and *NNA-BCP* distance refer to separations, the Laplacian $\nabla^2\rho(\mathbf{r}_a)$ and $\rho(\mathbf{r}_a)$ of the *NNA*, the Li-*NNA BCP* Laplacian $\nabla^2\rho(\mathbf{r}_b)$, $\rho(\mathbf{r}_b)$, total local energy density $H(\mathbf{r}_b)$, metallicity $\xi(\mathbf{r}_b)$, ellipticity ε are presented, atomic units are used.

Li_m^q	*BCP*	Li-*NNA*, *NNA-NNA*	*NNA-BCP*	$\rho(\mathbf{r}_a)$	$\nabla^2\rho(\mathbf{r}_a)$	$\rho(\mathbf{r}_b)$	$\nabla^2\rho(\mathbf{r}_b)$	$H(\mathbf{r}_b)$	$\xi(\mathbf{r}_b)$	ε
Li_2^-	Li1-*NNA*3	2.5118	0.5994	0.0112	-0.0084	0.0108	0.0027	-0.0020	4.0185	0.7007
Li_2^+	Li1-*NNA*3	2.9009	1.0041	0.0126	-0.0129	0.0118	-0.0014	-0.0027	-8.6544	0.0000
Li_3^-	Li1-*NNA*4	2.5475	0.5891	0.0102	-0.0078	0.0100	0.0003	-0.0017	34.5195	0.0000
	Li2-*NNA*4	3.1396	1.1750	0.0102	-0.0078	0.0094	0.0008	-0.0016	11.3060	0.0000
Li_3^+	Li1-*NNA*4	3.2136	1.4076	0.0163	-0.0108	0.0145	0.0058	-0.0022	2.5241	0.4534
Li_4^-	Li1-*NNA*5	3.7071	1.8340	0.0126	-0.0046	0.0107	0.0089	-0.0012	1.2021	0.0004
	Li2-*NNA*5	3.3094	1.4429	0.0126	-0.0046	0.0112	0.0092	-0.0012	1.2144	0.0293
Li_4^+	Li1-*NNA*5	2.8369	0.9524	0.0135	-0.0091	0.0129	0.0005	-0.0024	24.495	0.4407
	Li2-*NNA*5	3.5228	1.9004	0.0135	-0.0091	0.0120	0.0058	-0.0017	2.0904	7.2027
	*NNA*5-*NNA*6	4.8525	2.4223	0.0135	-0.0091	0.0124	-0.0067	-0.0026	-1.8334	0.5238
Li_5^-(1)	Li1-*NNA*6	3.0358	1.0864	0.0108	-0.0049	0.0102	0.0057	-0.0014	1.7901	53.735
	Li2-*NNA*8	3.2859	1.6854	0.0108	-0.0049	0.0104	0.0042	-0.0015	2.4640	30.150
	Li3-*NNA*6	3.2900	1.7529	0.0108	-0.0049	0.0104	0.0042	-0.0015	2.4891	76.761
	Li5-*NNA*8	3.2838	1.6673	0.0108	-0.0049	0.0104	0.0042	-0.0015	2.4609	24.607
	*NNA*6-*NNA*7	3.2519	1.6937	0.0108	-0.0049	0.0106	-0.0046	-0.0020	-2.2811	0.1865
Li_5^-(2)	Li1-*NNA*6	2.8111	0.9209	0.0120	-0.0083	0.0113	0.0040	-0.0017	2.7951	0.9123
	Li1-*NNA*7	3.9372	2.0942	0.0111	-0.0069	0.0096	0.0044	-0.0012	2.1724	6.2567
	Li3-*NNA*7	2.6195	0.6950	0.0111	-0.0069	0.0108	0.0021	-0.0016	5.1402	0.9162
	Li5-*NNA*6	4.3207	2.3870	0.0120	-0.0083	0.0093	0.0064	-0.0011	1.4511	11.755
	Li5-*NNA*7	3.5144	1.5819	0.0111	-0.0069	0.0096	0.0050	-0.0013	1.9373	2.5928
	*NNA*6-*NNA*7	4.9023	2.5679	0.0120	-0.0083	0.0098	-0.0041	-0.0017	-2.3948	0.7910
Li_5^-(3)	Li1-*NNA*6	3.9584	2.0731	0.0123	-0.0080	0.0099	0.0042	-0.0014	2.3835	0.2517
	Li1-*NNA*7	2.9561	1.0167	0.0111	-0.0091	0.0103	0.0008	-0.0018	12.375	0.0132
	Li3-*NNA*7	2.5716	0.6584	0.0111	-0.0091	0.0108	0.0016	-0.0018	6.7858	0.0018
	Li4-*NNA*6	2.3652	0.4579	0.0123	-0.0080	0.0121	0.0015	-0.0019	8.0873	1.2944
Li_5^+(1)	Li1-*NNA*6	2.9926	1.1886	0.0161	-0.0086	0.0147	0.0069	-0.0020	2.1284	0.0002
	Li2-*NNA*6	3.6472	1.8375	0.0161	-0.0086	0.0131	0.0110	-0.0016	1.1904	1.3937
	*NNA*6-*NNA*7	4.3451	2.1726	0.0161	-0.0086	0.0139	-0.0037	-0.0023	-3.8125	0.0002
Li_5^+(2)	Li1-*NNA*6	2.8325	1.0278	0.0160	-0.0119	0.0148	0.0053	-0.0023	2.8110	0.4312
	Li2-*NNA*6	4.1597	2.3032	0.0160	-0.0119	0.0118	0.0058	-0.0016	2.0206	0.2776

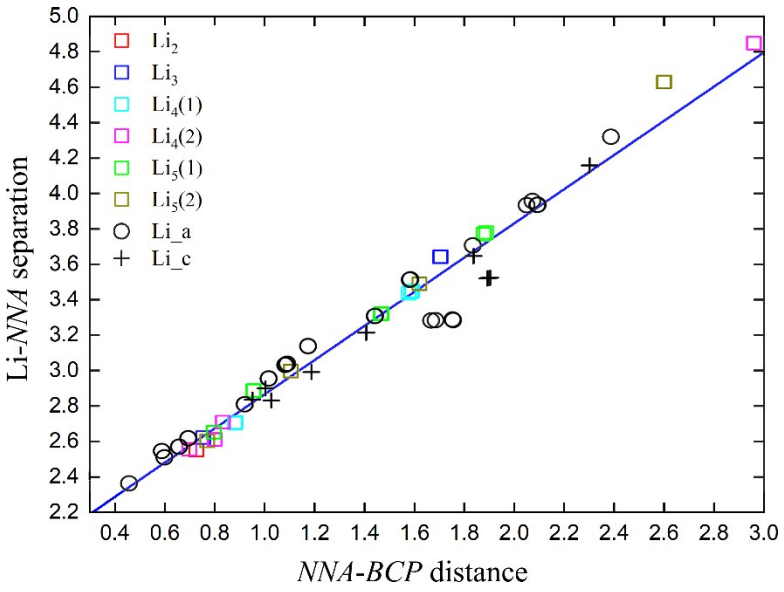

(a)

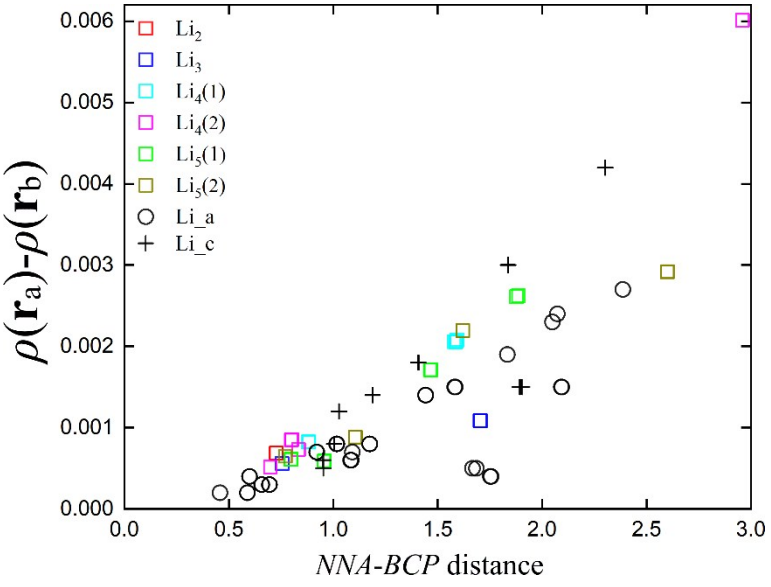

(b)

Figure S3. The linear fit between of the Li-*NNA BCP* separation and *NNA-BCP* distance, with slope = 0.964, intercept = 1.901 a.u., and correlation = 0.968 is presented in sub-figure **(a)**. The variation of the total electronic charge density difference $\rho(\mathbf{r}_a)$-$\rho(\mathbf{r}_b)$ of an *NNA* and neighboring bonded *BCP* and *NNA-BCP* distance for the Li_m^q (m = 2-5, q = 0, ±1) clusters is presented in sub-figure **(b)**, all units correspond to a.u., refer to **Table S3(iv)** of the main text.

4. Supplementary Materials S4.

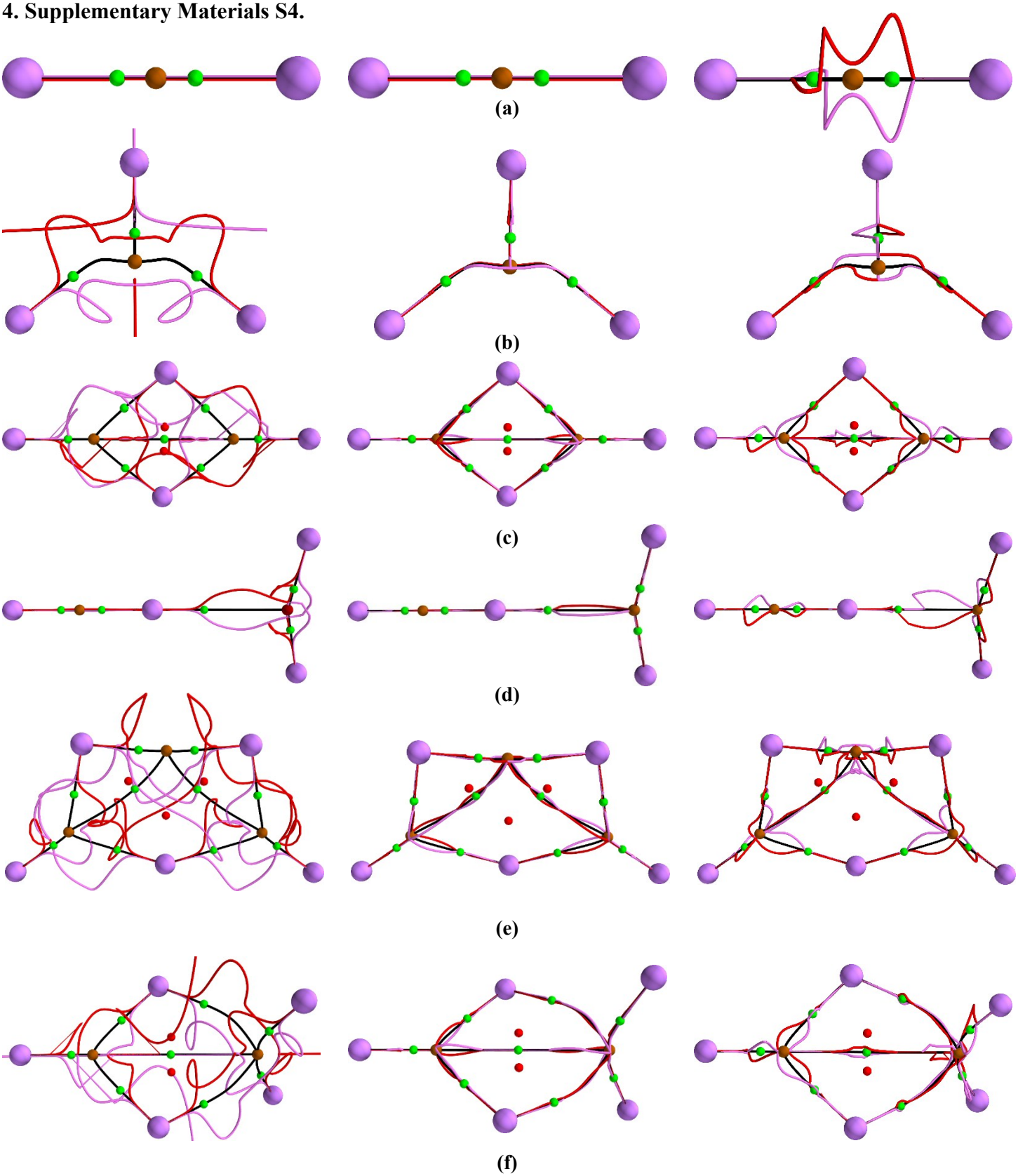

Figure S4(i). The QTAIM bond-path framework sets $B = \{q,q',r\}$, $B_\sigma = \{q_\sigma,q_\sigma',r\}$ and $B_{\sigma H} = \{q_{\sigma H},q_{\sigma H}',r\}$ paths for the Li_m (m = 2-5) are presented in the left, middle and right panels in sub-figures **(a-f)** respectively. See caption of **Figure 1** for further details.

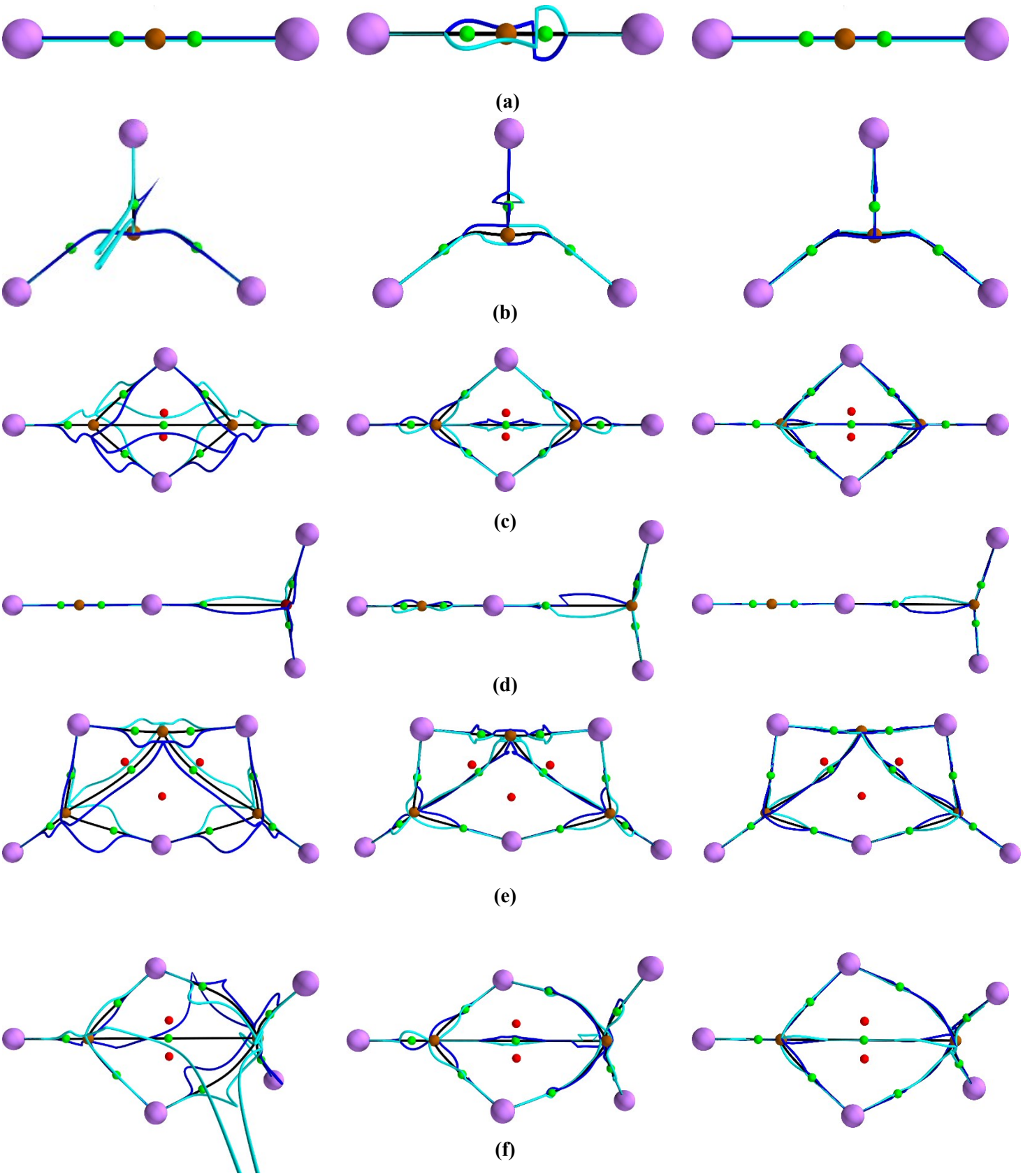

Figure S4(ii). The QTAIM bond-path framework sets $\mathsf{B} = \{\boldsymbol{p},\boldsymbol{p}',\boldsymbol{r}\}$, $\mathsf{B}_{\sigma} = \{\boldsymbol{p}_{\sigma},\boldsymbol{p}_{\sigma}',\boldsymbol{r}\}$and $\mathsf{B}_{\sigma\mathrm{H}} = \{\boldsymbol{p}_{\sigma\mathrm{H}},\boldsymbol{p}_{\sigma\mathrm{H}}',\boldsymbol{r}\}$ paths for the Li_m (m = 2-5) are presented in the left, middle and right panels in sub-figures **(a-f)** respectively. See caption of **Figure 1** for further details.

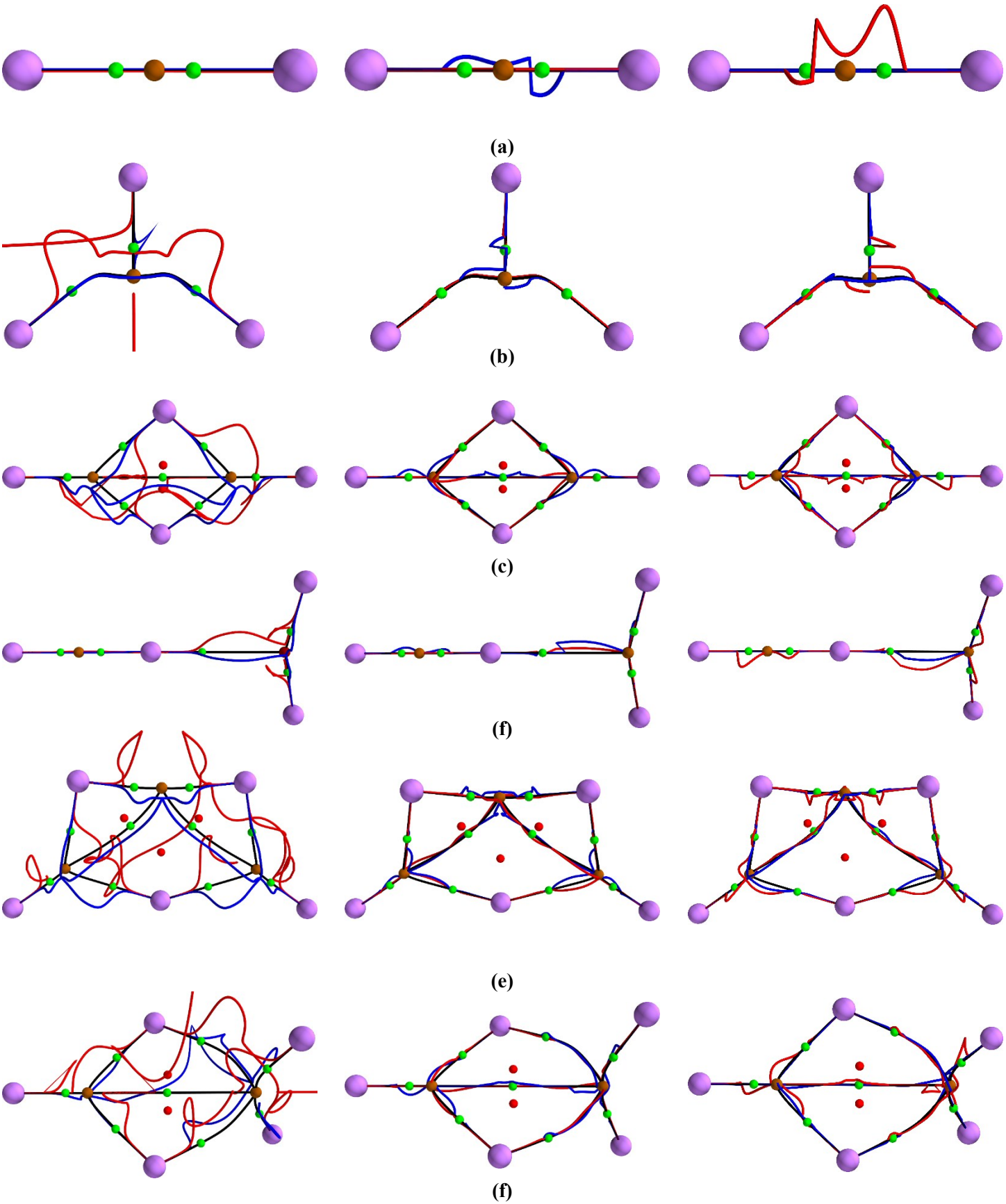

Figure S4(iii). The QTAIM bond-path framework sets $B = \{p,q,r\}$, $B_{\sigma} = \{p_{\sigma},q_{\sigma},r\}$ and $B_{\sigma H} = \{p_{\sigma H},q_{\sigma H},r\}$ paths for the Li_m (m = 2-5) are presented in the left, middle and right panels in sub-figures **(a-f)** respectively. See caption of **Figure 1** for further details.

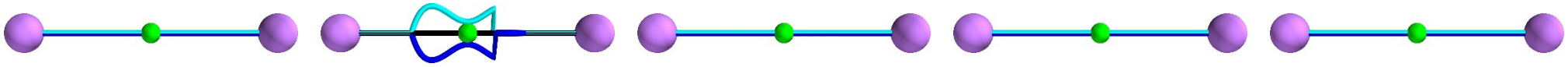

(a)

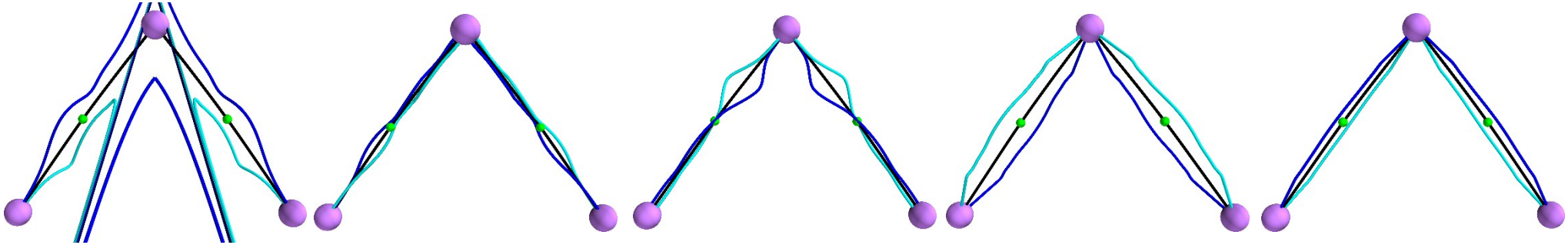

(b)

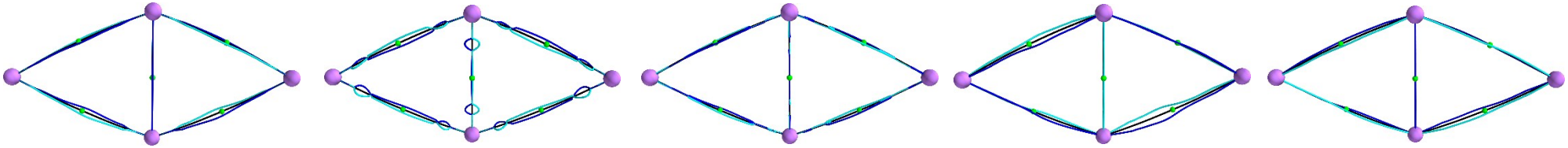

(c)

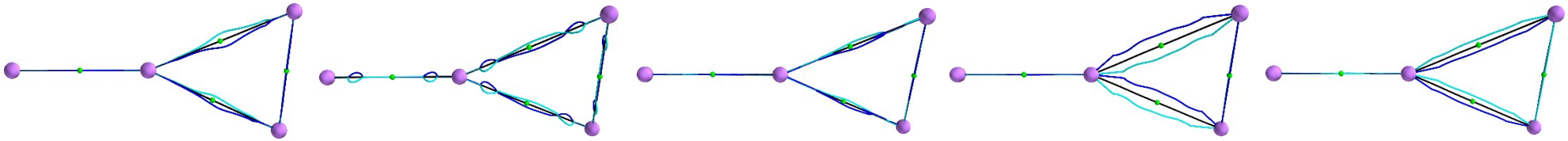

(d)

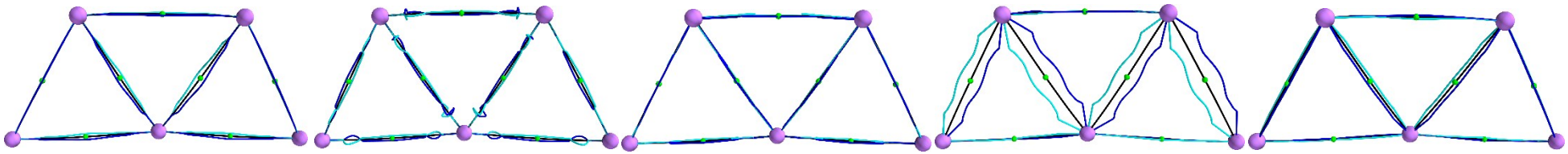

(e)

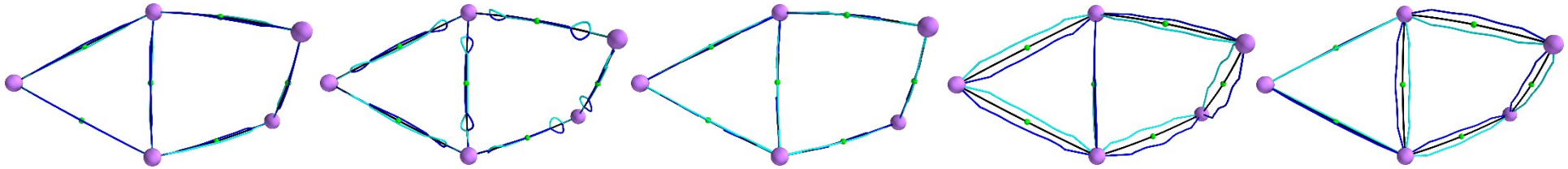

(f)

Figure S4(iv). The Ehrenfest bond-path framework sets $\mathsf{B} = \{\boldsymbol{p},\boldsymbol{p}',\boldsymbol{r}\}$, $\mathsf{B}_{\sigma} = \{\boldsymbol{p}_{\sigma},\boldsymbol{p}_{\sigma}',\boldsymbol{r}\}$, $\mathsf{B}_{\sigma H} = \{\boldsymbol{p}_{\sigma H},\boldsymbol{p}_{\sigma H}',\boldsymbol{r}\}$, $\mathsf{B}_{Fa} = \{\boldsymbol{p}_{\mathbf{Fa}},\boldsymbol{p}_{\mathbf{Fa}}',\boldsymbol{r}\}$ and $\mathsf{B}_{Fb} = \{\boldsymbol{p}_{\mathbf{Fb}},\boldsymbol{p}_{\mathbf{Fb}}',\boldsymbol{r}\}$ paths for the Li_m (m = 2-5) are presented from left to right panels in sub-figures **(a-f)** respectively. The filter path with range 0.6 is applied to B_{Fa} and B_{Fb}. See the caption of **Figure 1** of the main text for further details.

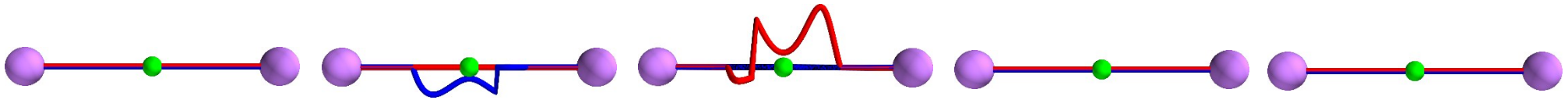

(a)

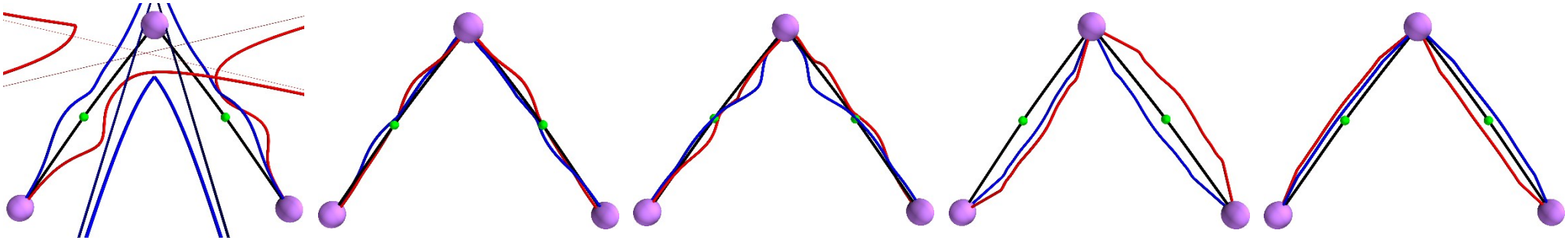

(b)

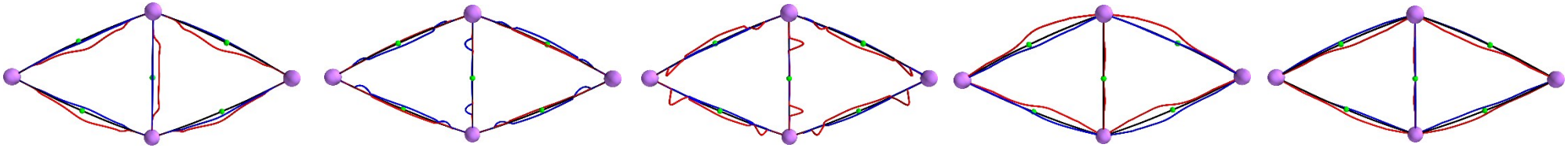

(c)

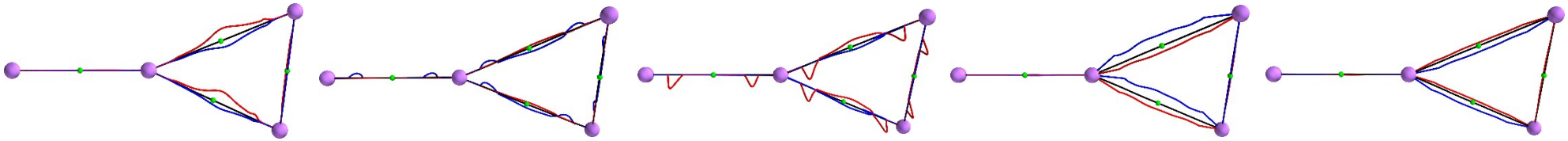

(d)

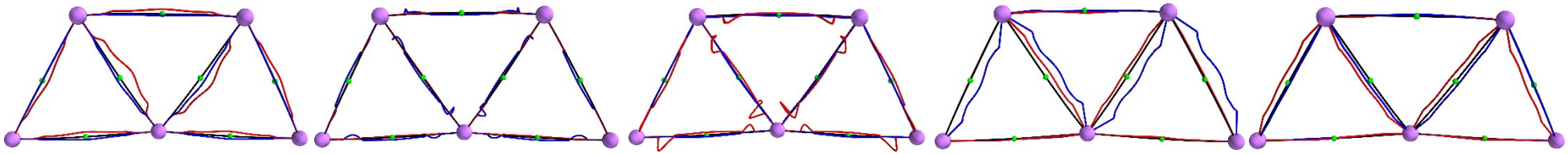

(e)

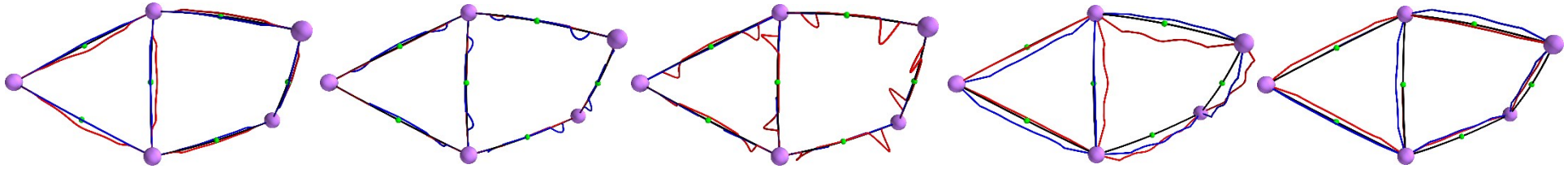

(f)

Figure S4(v). The Ehrenfest bond-path framework sets $\mathsf{B} = \{\boldsymbol{p},\boldsymbol{q},\boldsymbol{r}\}$, $\mathsf{B}_{\sigma} = \{\boldsymbol{p}_{\sigma},\boldsymbol{q}_{\sigma},\boldsymbol{r}\}$, $\mathsf{B}_{\sigma H} = \{\boldsymbol{p}_{\sigma H},\boldsymbol{q}_{\sigma H},\boldsymbol{r}\}$, $\mathsf{B}_{Fa} = \{\boldsymbol{p}_{\mathbf{Fa}}, \boldsymbol{q}_{\mathbf{Fa}}, \boldsymbol{r}\}$ and $\mathsf{B}_{Fb} = \{\boldsymbol{p}_{\mathbf{Fb}}, \boldsymbol{q}_{\mathbf{Fb}}, \boldsymbol{r}\}$ paths for the Li_m (m = 2-5) are presented from left to right panels in sub-figures **(a-f)** respectively. Filter path range 0.6 is applied on B_{Fa} and B_{Fb} See caption of **Figure 1** for further details.

5. Supplementary Materials S5.

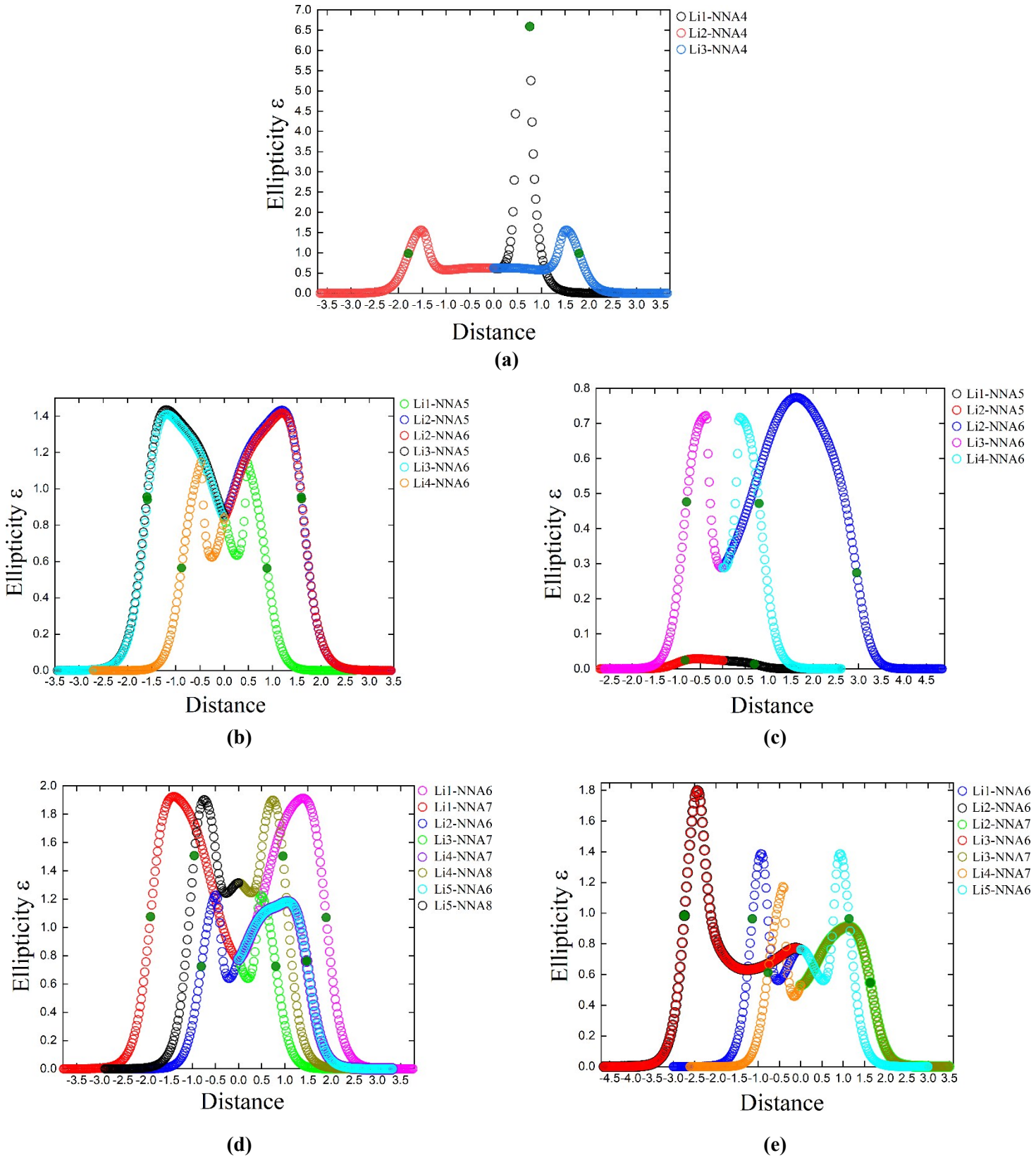

Figure S5(i). The variation of ellipticity ε profile with distance along the Li-*BCP*-*NNA*-*BCP*-Li separation in a.u. for Li_m (m = 3-5) clusters are presented on the QTAIM molecular graphs in sub-figures **(a-e)** respectively, see the caption of **Figure 2** of the main text for further information.

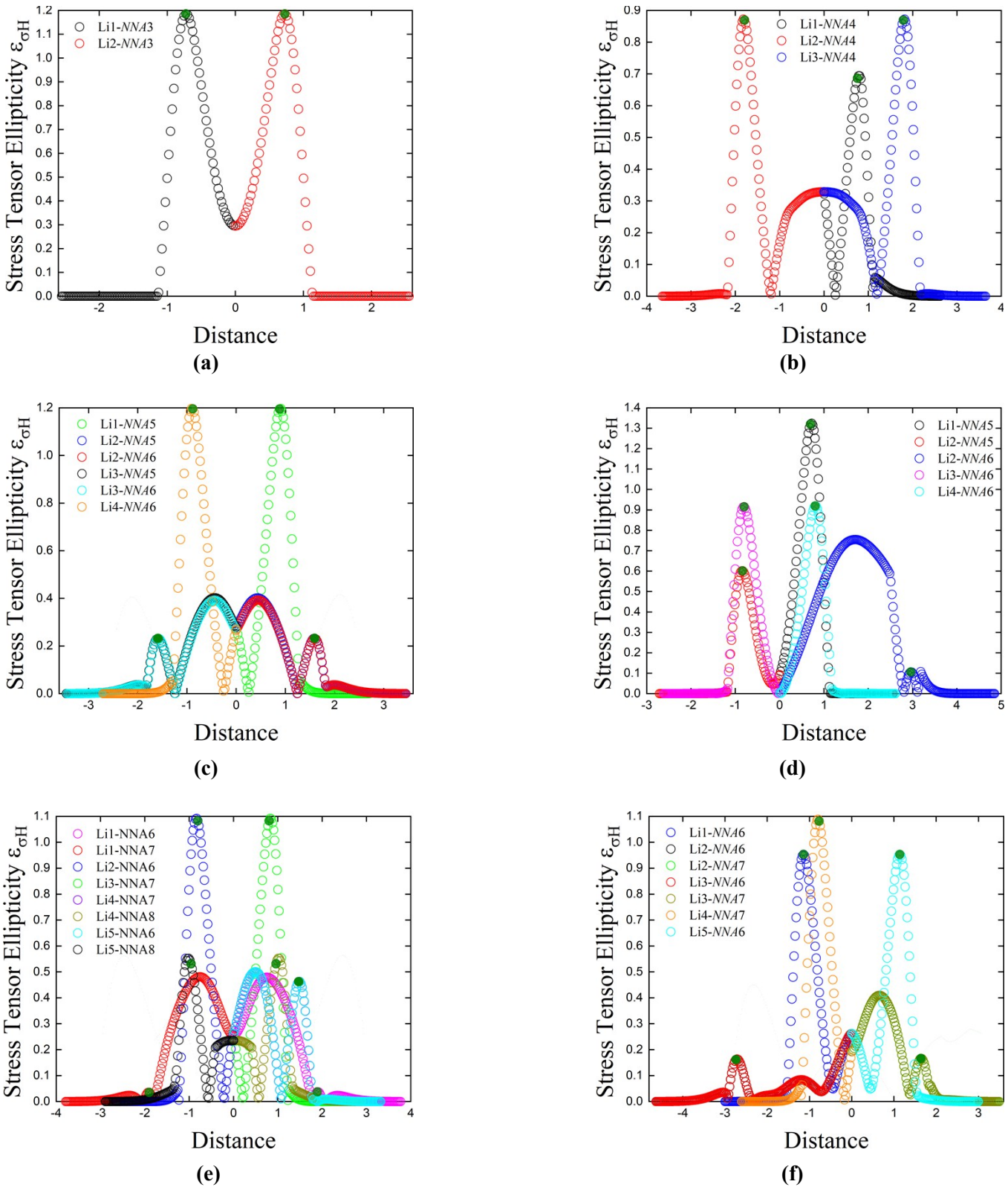

Figure S5(ii). The variation of the stress tensor ellipticity $\varepsilon_{\sigma H}$ profile with distance along the Li-*BCP*-*NNA*-*BCP*-Li separation in a.u. Li_m (m = 2-5) clusters are presented on the QTAIM molecular graphs in sub-figures **(a-f)** respectively, see caption of **Figure 2** of the main text for further information.

6. Supplementary Materials S6.

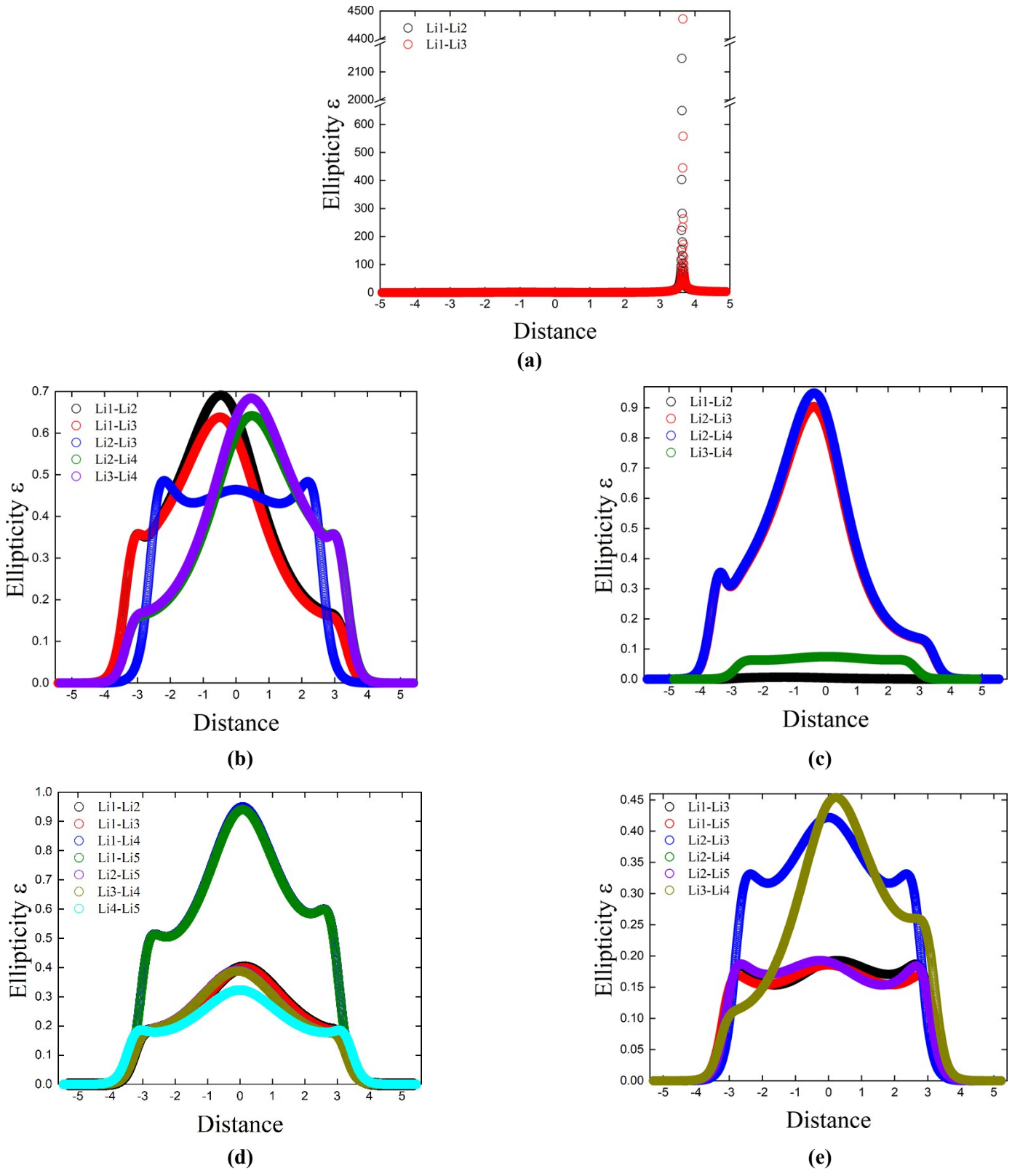

Figure S6(i). The variation of ellipticity $\varepsilon = (|\lambda_1|/|\lambda_2|) - 1$ with distance along the Li-Li separation in a.u. for Li_m (m = 3-5) are presented on the Ehrenfest Force **F**(**r**) molecular graphs in sub-figures **(a-e)** respectively. *BCP* is located at a distance = 0.0 a.u.

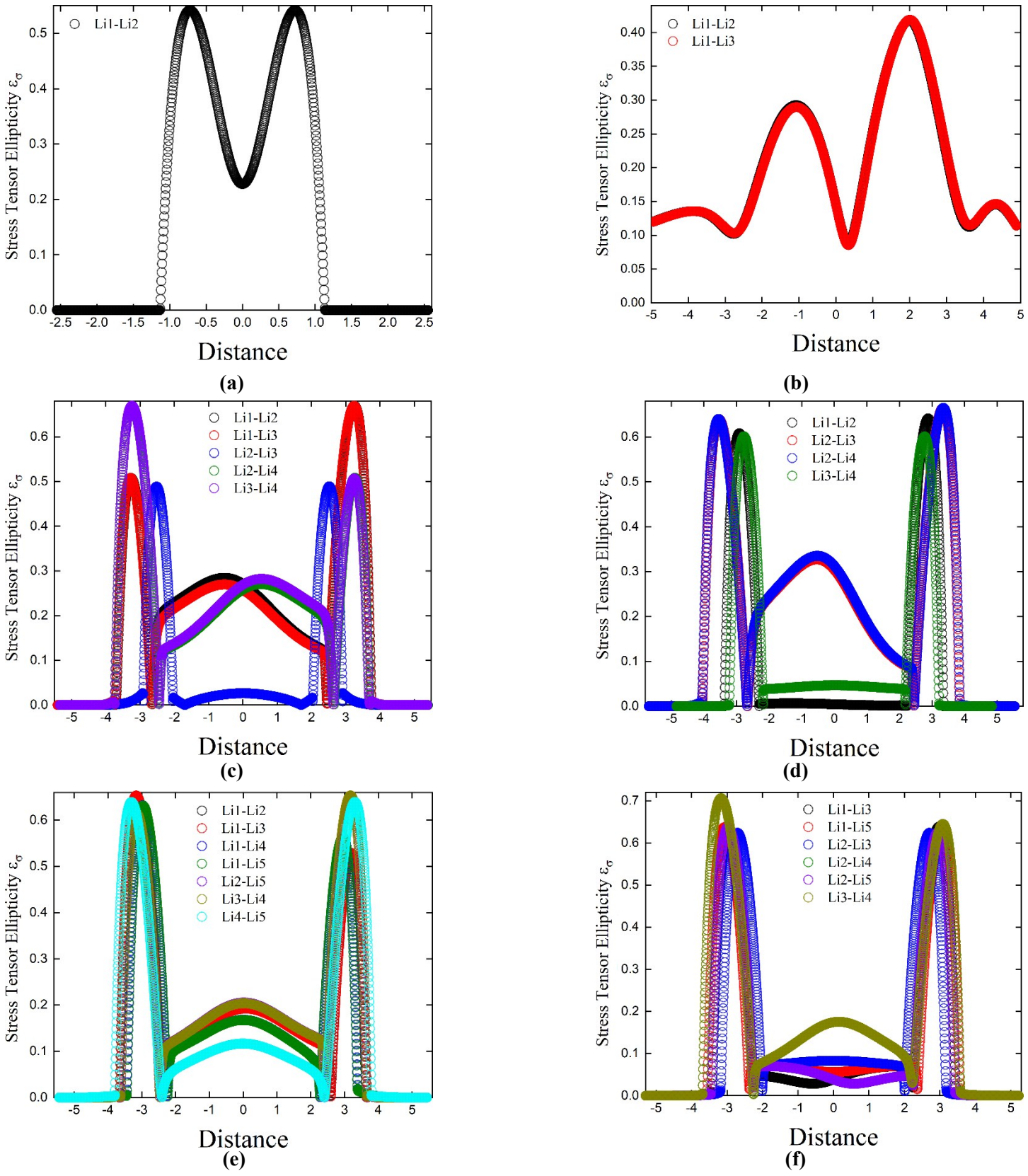

Figure S6(ii). The variation of stress tensor ellipticity $\varepsilon_\sigma = (|\lambda_{2\sigma}|/|\lambda_{1\sigma}|) - 1$ with distance along the Li-Li separation in a.u. for Li_m (m = 2-5) are presented on the Ehrenfest Force **F**(**r**) molecular graphs in sub-figures **(a-f)** respectively. See caption of **Figure S6(i)** for further details.

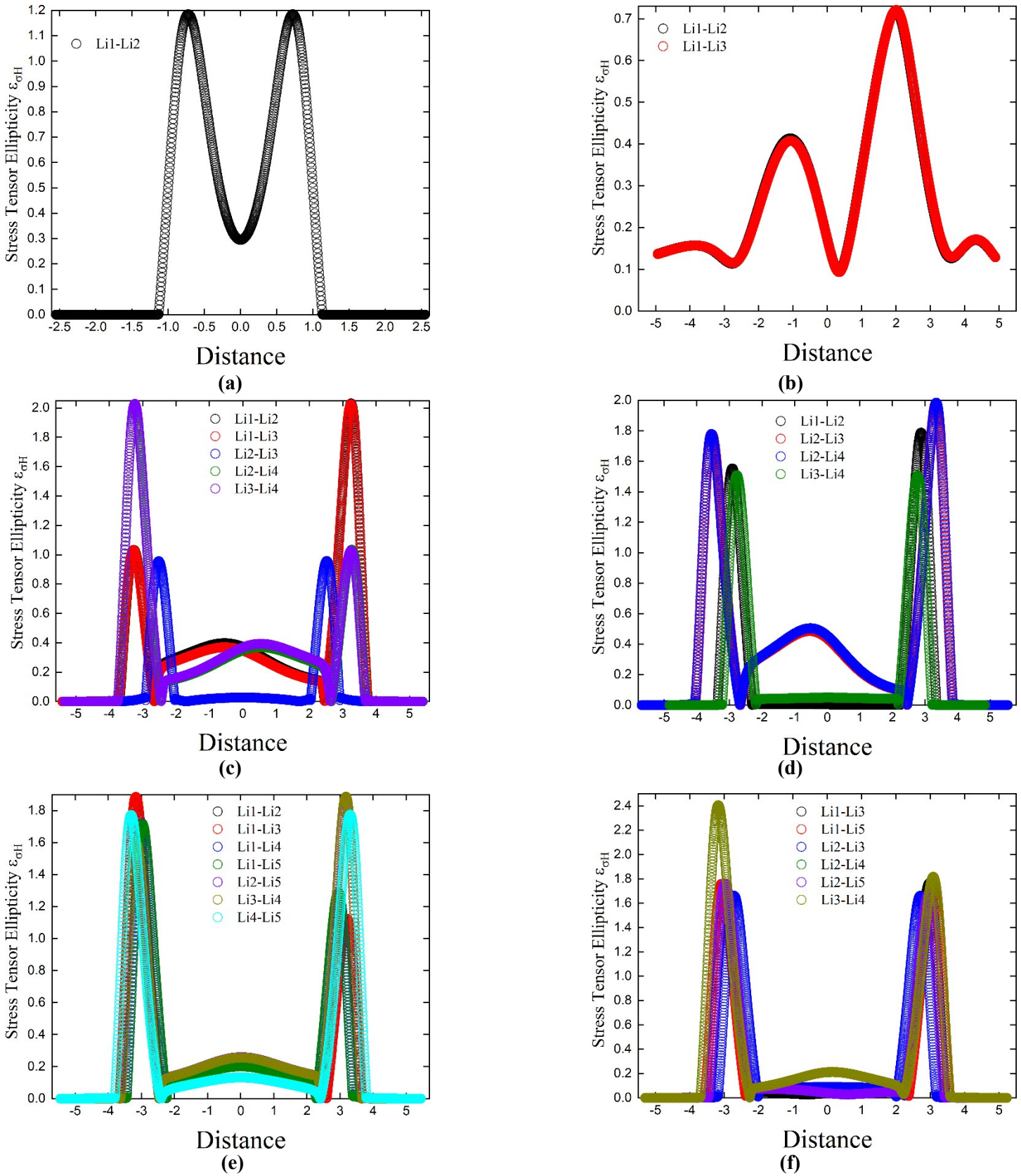

Figure S6(iii). The variation of stress tensor hessian ellipticity $\varepsilon_{\sigma H} = (|\lambda_{1\sigma}|/|\lambda_{2\sigma}|) - 1$ with distance along the Li-Li separation in a.u. for Li_m (m = 2-5) are presented on the Ehrenfest Force **F**(**r**) molecular graphs in sub-figures **(a-f)** respectively. See caption of **Figure S6(i)** for further details.

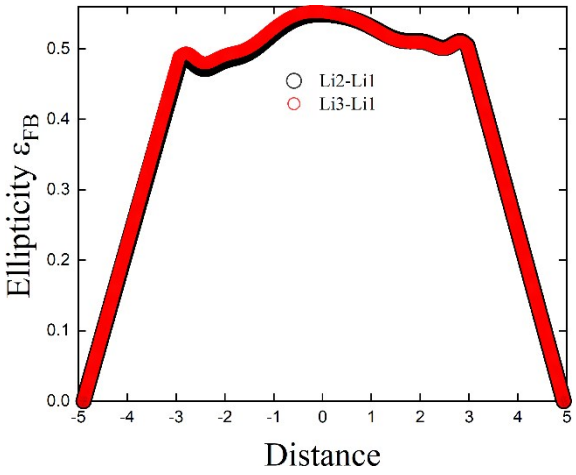

(a)

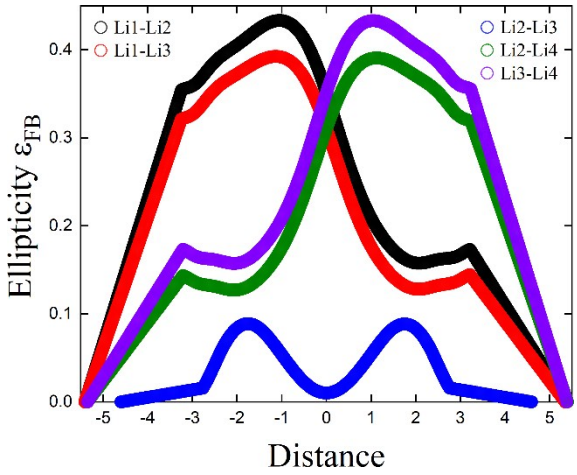

(b)

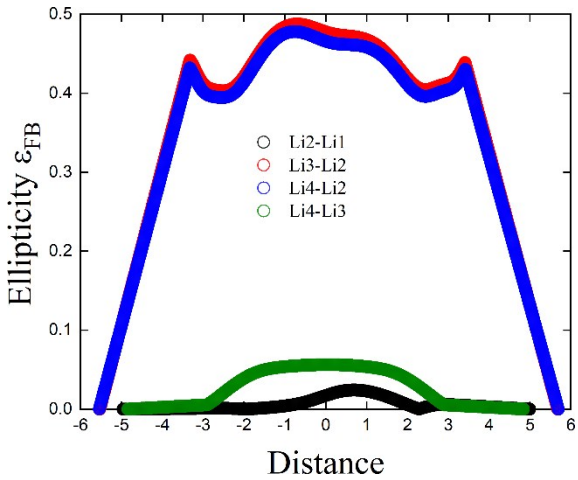

(c)

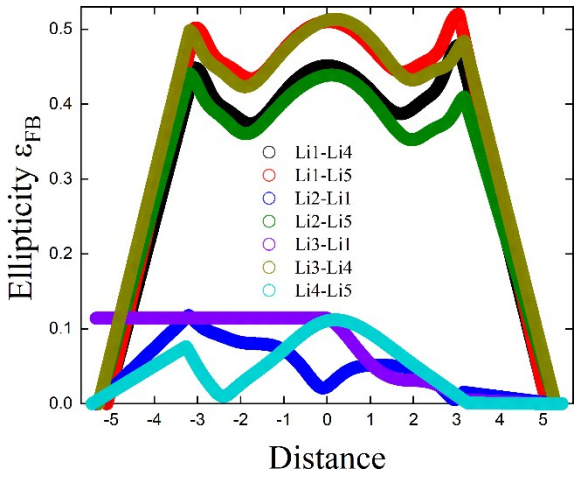

(d)

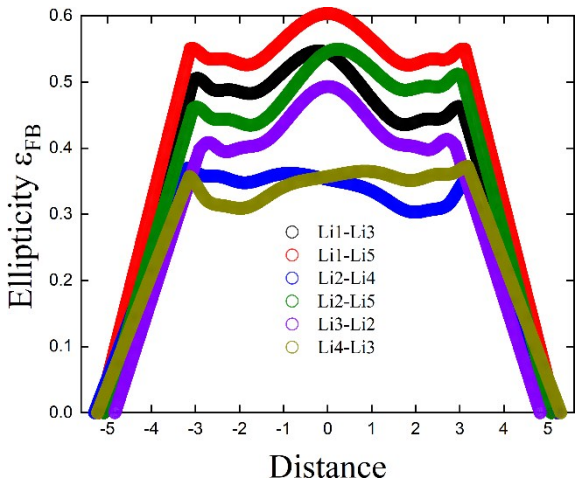

(e)

Figure S6(iv). The variation of ellipticity $\varepsilon_{FB} = (|\lambda_{2F}|/|\lambda_{1F}|) - 1$ with distance along the Li-Li separation in a.u. for Li_m (m = 3-5) are presented on the Ehrenfest Force **F**(**r**) molecular graphs in sub-figures **(a-e)** respectively. See caption of **Figure S6(i)** for further details.

7. Supplementary Materials S7.

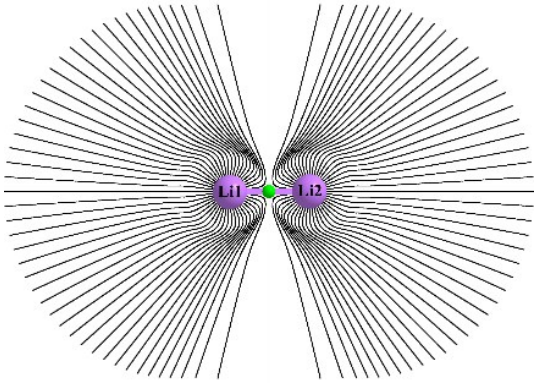

(a)

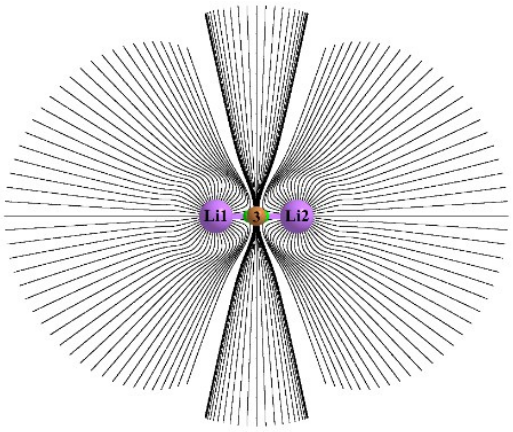

(b)

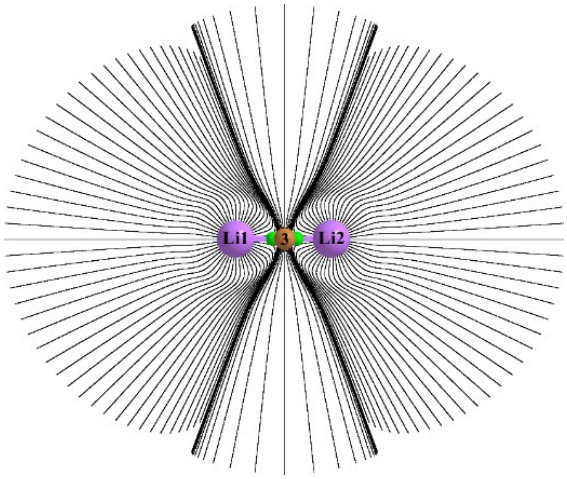

(c)

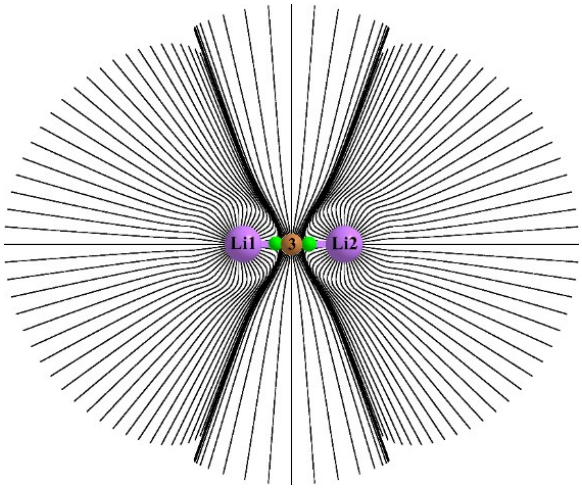

(d)

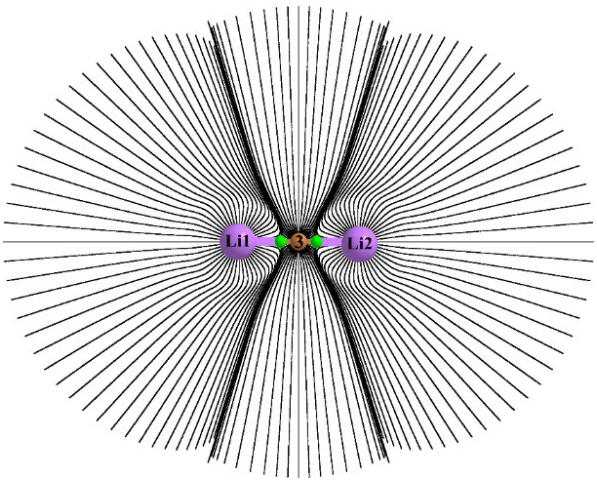

(e)

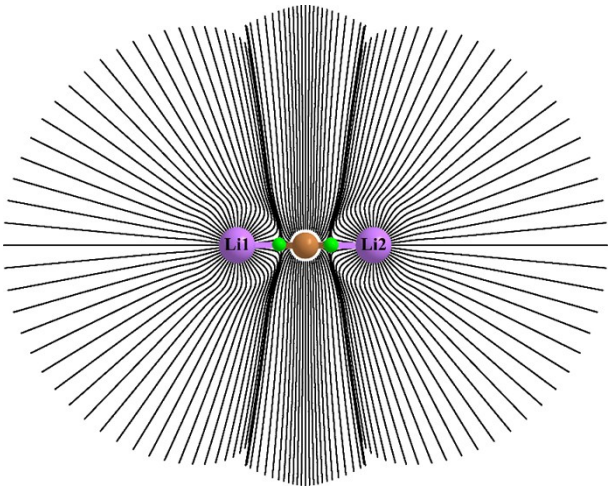

(f)

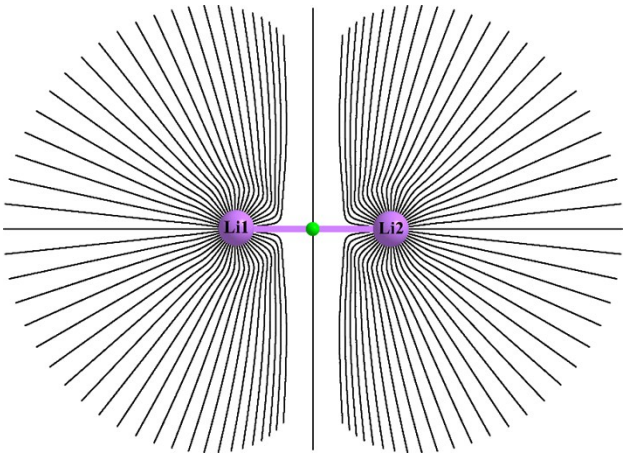

(g)

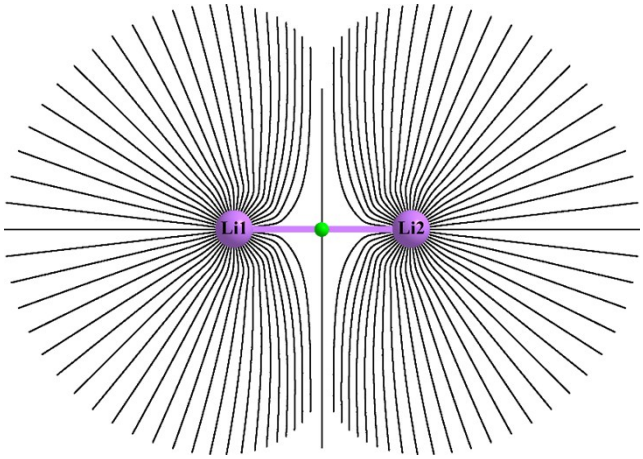

(h)

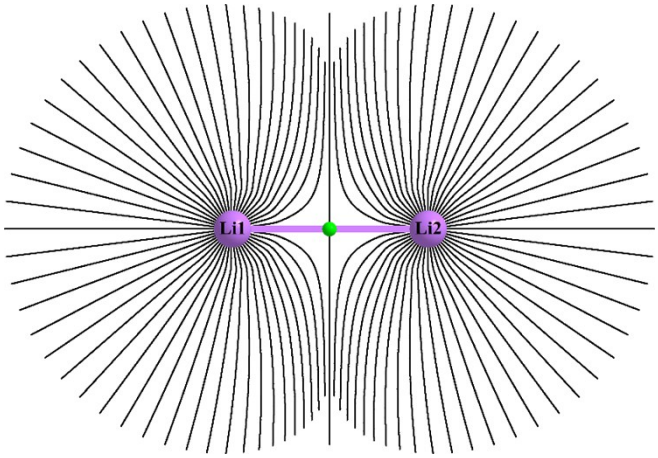

(i)

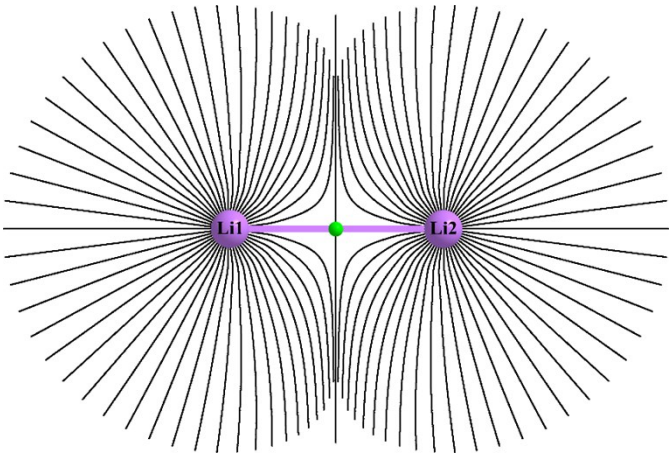

(j)

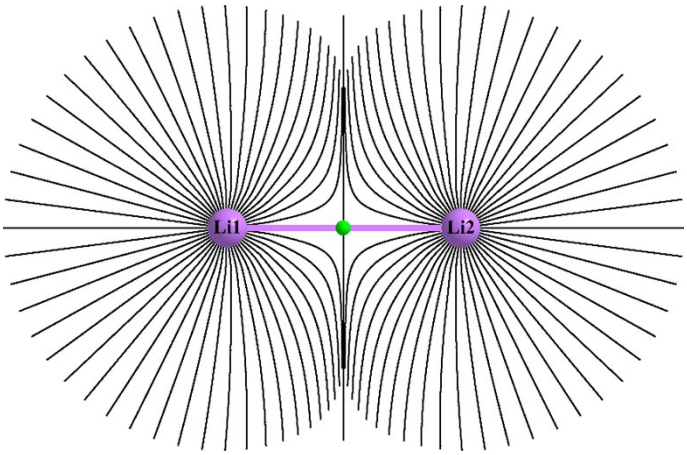

(k)

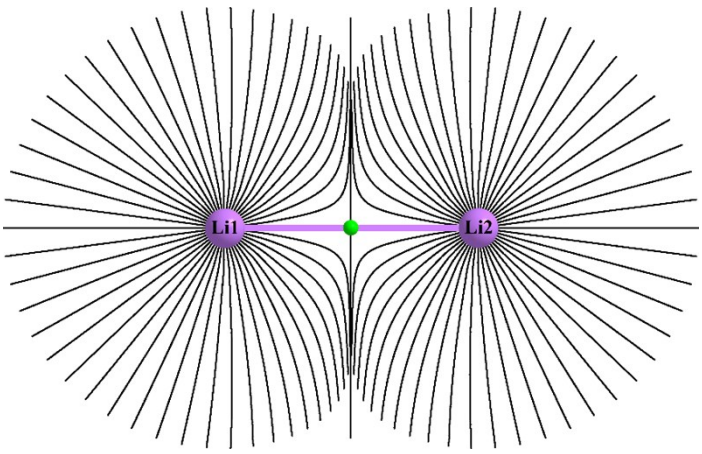

(l)

Figure S7(i). The QTAIM trajectory maps are superimposed onto the corresponding molecular graphs for Li_2. The purple spheres represent the lithium nuclear critical points (*NCP*s), the brown and green represent QTAIM non–nuclear attractors (*NNA*s) and bond critical points (*BCP*s) respectively. Figures **(a-l)** are corresponding to **Table 1**.

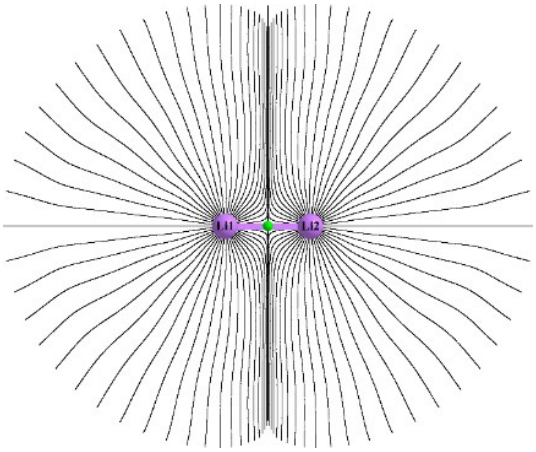

(a)

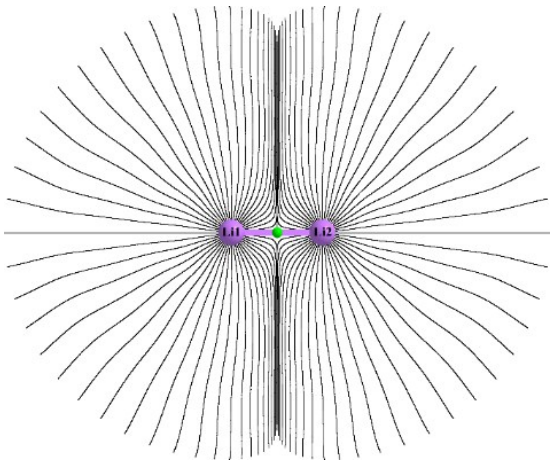

(b)

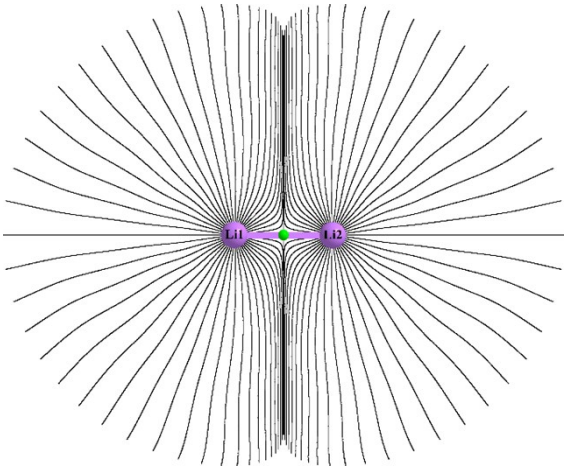

(c)

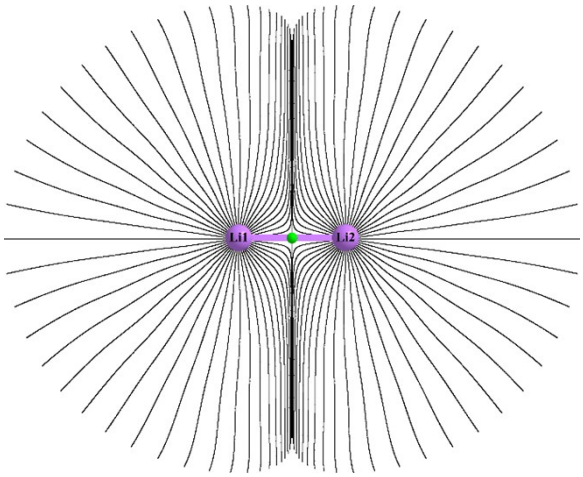

(d)

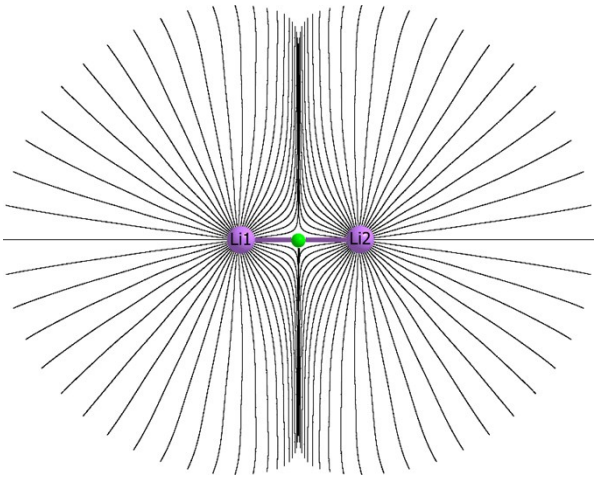

(e)

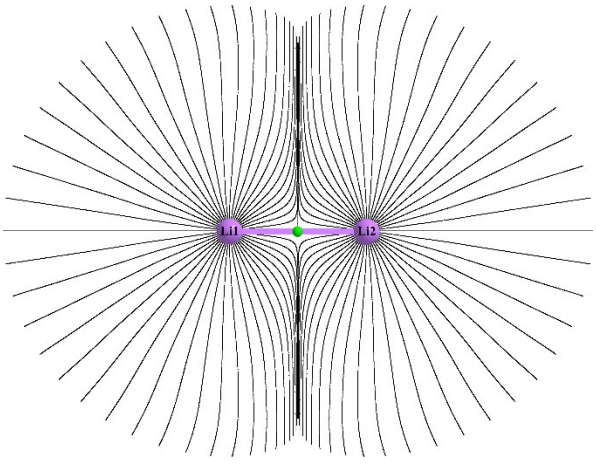

(f)

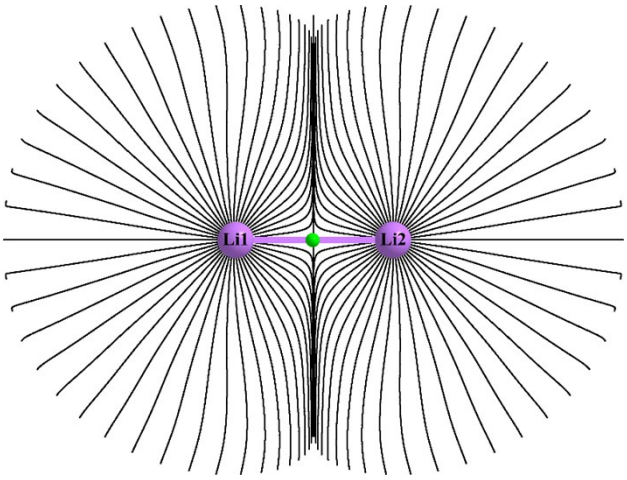

(g)

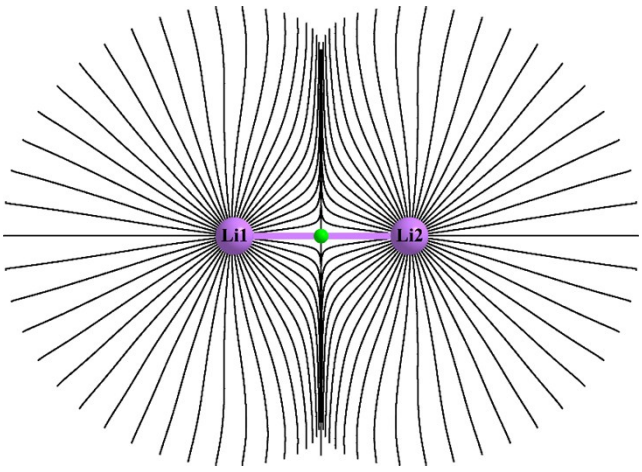

(h)

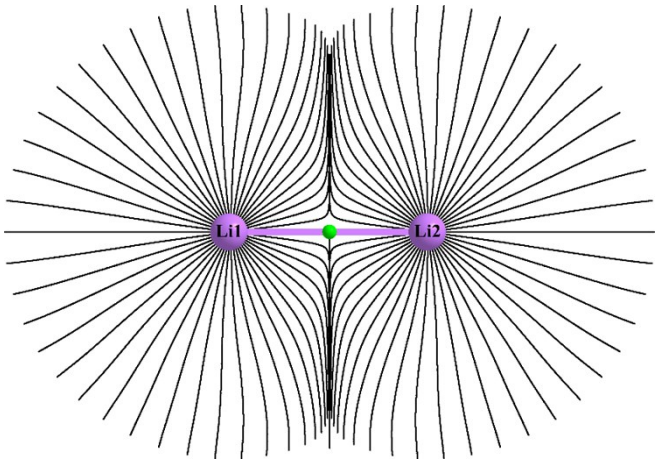

(i)

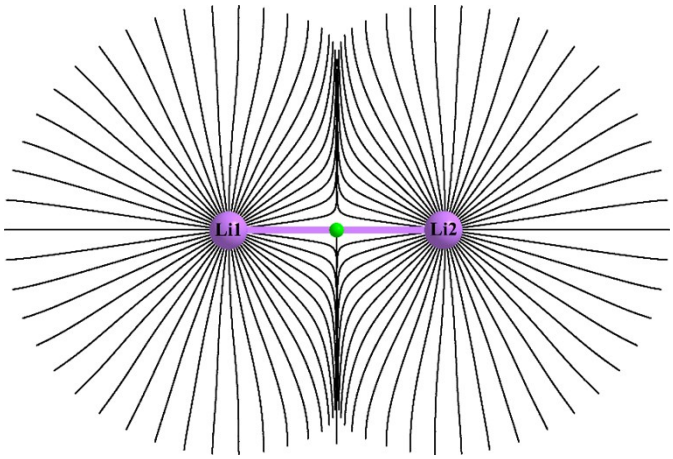

(j)

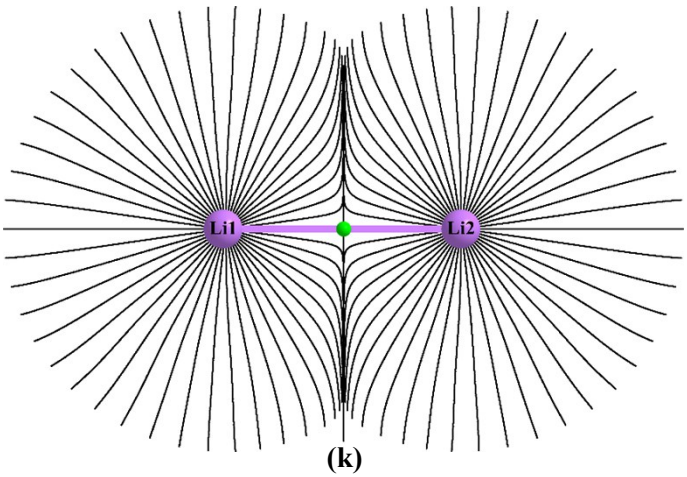

(k)

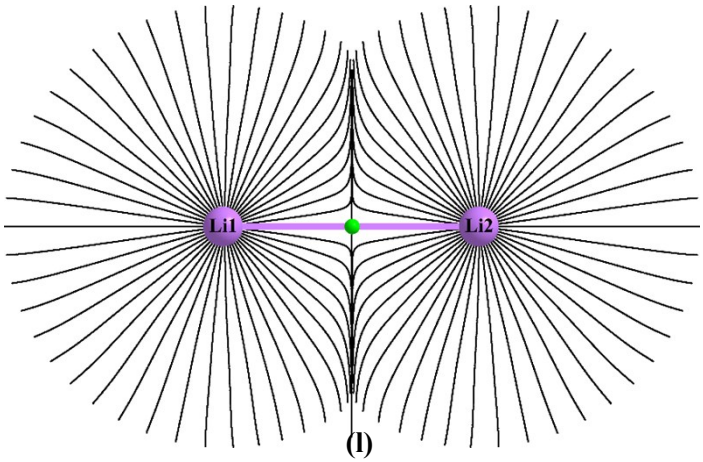

(l)

Figure S7(ii). The Ehrenfest Force **F**(**r**) trajectory maps are superimposed onto the corresponding molecular graphs for Li_2. The purple and green spheres represent the lithium nuclear critical points (*NCP*s) and bond critical points (*BCP*s) respectively. Figures **(a-l)** are corresponding to **Table 2**.